Whole Range of Chain Dynamics in Entangled Polystyrene Melts Revealed from Creep Compliance: Thermorheological Complexity between Glassy-Relaxation Region and Rubber-to-Fluid Region. 1

Y.-H. Lin*

Department of Applied Chemistry, National Chiao Tung University, Hsinchu, Taiwan

Received: August 19, 2004; In Final Form: May 27, 2005

The rubber(like)-to-fluid region of the creep compliance $J(t)$ results reported by Plazek of two nearly monodisperse polystyrene melts in the entanglement region have been quantitatively analyzed in terms of the extended reptation theory (ERT), giving the frictional factor K $(= \zeta \langle b^2 \rangle / kT\pi^2 m^2)$ in quantitative agreement with the values obtained previously from analyzing the relaxation modulus $G(t)$ line shapes as well as calculated from the viscosity and diffusion data—a quantity shown independent of molecular weight as expected from the theory. Using the successful description of $J(t)$ in terms of ERT in the rubber(like)-to-fluid region as the reference frame in time, the glassy-relaxation process $\mu_G(t)$ that occurs in the small-compliance short-time region of $J(t)$ can be studied in perspective. As shown from the analysis in terms of a stretched exponential form for $\mu_G(t)$ incorporated into ERT, the temperature dependence of the *energetic interactions-derived* $\mu_G(t)$ process being stronger in a simple manner than that of the *entropy-derived* ERT processes accounts fully for the uneven thermorheological complexity occurring in $J(t)$ as initially observed by Plazek. When the results of analysis being displayed in the $G(t)$ form, the relative roles of the energetic interactions-derived dynamic process and the entropy-derived ones in polystyrene are clearly revealed. It is shown that at the calorimetric glass transition temperature (T_g) the contribution from energetic interactions among segments to $G(t)$ at the time scale of the highest Rouse−Mooney normal mode greatly exceeds that derived from entropy, indicating vitrification at the Rouse-segmental level. At the same time the Rouse−Mooney normal modes provide an internal yardstick for estimating the characteristic length scale of a polymer at T_g, giving ∼3 nm for polystyrene. On the basis of the obtained results, the basic mechanism for the thermorheological complexity occurring in polystyrene is analyzed. It is shown that this basic mechanism should be also responsible for the breakdown of the Stoke−Einstein equation in relating the translational diffusion constant and viscosity as observed in glass-forming liquids, such as OTP and TNB, in approaching T_g from above.

1. Introduction

Because of the large number of atoms and degrees of freedom in a chain molecule, a polymer is rich in its dynamics, with its relaxation-time distribution easily covering many decades. For example, the time domain of the polystyrene sample with M_w $= 1.22 \times 10^5$ whose creep compliance $J(t)$ is analyzed in this study stretches over nine decades. In general, a slow mode of dynamics corresponds to a large length scale in the chain; a fast one to a short one. It is generally understood[1] that the long-time region of the relaxation modulus $G(t)$ is sensitive to the molecular weight, coupled with entanglement; and the short-time region, with the modulus approaching that of the glass state, is sensitive to the local energetic interactions among segments. In between, there are the transition and plateau zones, which are closely related to chain entanglement (for instance, from the plateau modulus G_N one can obtain the entanglement molecular weight, $M_e = 4\rho RT/5G_N$). Over the years, it has been a challenge to understand the dynamics corresponding to different length scales at a molecular level and even more so to study all of them consistently in a unified way. To analyze consistently the whole range of chain dynamics in a unified way requires a theory that has interfaced dynamics at different length scales seamlessly. In the past two decades, the constitutive

molecular models have been developed and tested. This paper represents a further progress, showing an application of what has been developed and discussing the implications of the obtained result, particularly in the understanding of the glass transition. It has been shown[2−6] that the Doi−Edwards theory,[7] describing the entanglement effect in terms of reptation of the primitive chain, has laid a solid foundation and that the extended reptation theory (ERT),[5,8] developed by incorporating intramolecular Rouse-type motions into the Doi−Edwards theory, is quantitatively successful. As they have been studied in detail elsewhere, the dynamic processes in ERT will be described only briefly here. This paper will first show mainly two aspects: (1) The validity of ERT is again confirmed by the analysis of the creep compliance $J(t)$ as evidenced by the obtained frictional factor K $(= \zeta \langle b^2 \rangle / kT\pi^2 m^2$, where ζ, b, and m are the friction constant, length and mass of the Rouse segment) being in quantitative agreement with those obtained from analyzing the data of relaxation modulus, viscosity, and diffusion and shown to be independent of the molecular weight as expected from the theory. (2) The quantitative description of the rubber(like)-to-fluid (or large-compliance/long-time) region of $J(t)$ in terms of ERT can be used as the *reference frame* in time, with respect to which the small-compliance/short-time region of $J(t)$ can be analyzed in perspective, giving microscopic information about

* E-mail: yhlin@mail.nctu.edu.tw.

Whole Range of Chain Dynamics

J. Phys. Chem. B, Vol. 109, No. 37, 2005 **17655**

the dynamics closely related to the glass transition from a totally new viewpoint.

Developed on the basis of the Doi−Edwards theory, ERT gives the relaxation modulus:

$$G(t) = \frac{4\rho RT}{5M_e}F(t)\Big[1 + \frac{1}{4}\mu_X(t/\tau_x)\Big][\sqrt{M_e/M}\mu_B(t/\tau_B) +$$

$$(1 - \sqrt{M_e/M})\mu_C(t/\tau_C)] \quad (1)$$

with

$$F(t) = 1 + \mu_A(t/\tau_A) \quad (2)$$

where $\mu_A(t)$ represents the Rouse−Mooney modes of motion of an entanglement strand with both ends fixed (in the short-time region, the entanglement links are regarded as fixed, cross-linked points because the chain has not had the chance to slip through the links yet. In this paper, the region where the $\mu_A(t)$ process is applicable will be referred to as the Rouse−Mooney rubber region or simply as the rubber region. Note: The $\mu_A(t)$ process has often been used to represent the so-called transition zone in the literature.[1] Experimentally, the transition zone should include a large portion of the glassy-relaxation process, which will be studied in this paper); $\mu_X(t)$, the chain slippage through entanglement links to equilibrate the uneven tension along the primitive chain; $\mu_B(t)$, the primitive-chain contour-length fluctuation; and $\mu_C(t)$, the reptation motion corrected for the chain length-fluctuation effect. For easy explanation as well as for referring to the research results as described in the literature, the time region that covers the $\mu_X(t)$, $\mu_B(t)$, and $\mu_C(t)$ processes is grossly referred to as the rubberlike-to-fluid region, and that covers all the four processes $\mu_A(t)$, $\mu_X(t)$, $\mu_B(t)$, and $\mu_C(t)$ as the rubber-to-fluid region (see the note in ref 9).[9] The relaxation times of these different processes are each expressed as a product of the frictional factor K and a structural factor. We refer the functional forms of the four relaxation processes and their respective characteristic (relaxation) times to the previous publications[2−5,8] but point out that, normalizing (dividing) all the relaxation times by the relaxation time of the first mode of $\mu_A(t)$, τ_A^1, the whole $G(t)$ can be expressed as a universal function of the normalized molecular weight M/M_e. In this paper, all the relaxation times are expressed in the unit of second and the molecular masses: M, M_e, and m in the unit of Da; thus, the frictional factor K has the unit of s/Da^2.

ERT has successfully predicted the characteristics of transformation with molecular weight of the $G(t)$ line shape of the nearly monodisperse sample system and the molecular-weight dependence of the zero-shear viscosity η and the steady-state compliance (J_e^0) and their respective transition points M_c and M_c'.[2−6,8] However, the analysis of the relaxation modulus or viscoelastic spectrum in terms of ERT has been limited to the modes of motion associated with length scales above that of a Rouse segment. The main reason is that the smallest structural unit in ERT is the Rouse segment, whose molecular weight (m) is estimated to be about 850 for polystyrene.[10−18] Experimental limitation also prevents the modes of motion faster than that of a single Rouse segment from being studied. The measurement of $G(t)$ in the high modulus region is often limited by the lack of a compliance-free transducer. Thus, in the previous studies of polystyrene,[2−5,8] the highest modulus that could be studied was about 10^7 dyn/cm^2, which is of the magnitude a little smaller than that corresponding to $m = 850$.[12−14] On the other hand, the creep experiment based on the use of the frictionless magnetic bearing by Plazek allowed the creep compliance $J(t)$

as small as $\sim10^{-10}$ cm^2/dyn to be measured accurately.[19,20] These small measurable compliance values correspond to the large modulus values of reciprocal magnitude. As ERT can be used to analyze quantitatively the relaxation modulus $G(t)$ of magnitude smaller than $\sim10^7$ dyn/cm^2, it is expected to describe well the creep compliance $J(t)$ in the large-compliance/long-time region. From the analyses of the relaxation modulus curves of a series of nearly monodisperse polystyrene samples of different molecular weights in terms of ERT, the obtained frictional factor K is shown to be independent of molecular weight. This result is critically important to ERT, indicating that the functional forms of the dynamic processes as arranged in eqs 1 and 2 as well as the structural factors of their respective relaxation times are accurately given. Thus, with both the molecular weight and entanglement molecular weight M_e known (M_e determined independently from the plateau modulus $G_N = 4\rho RT/5M_e$), the analysis of the large-compliance/long-time (rubber(like)-to-fluid) region of $J(t)$ in terms of ERT is boiled down to the determination of the single parameter K.[21]

The small-compliance/short-time region of $J(t)$ reflects the fast local segmental motions, which are much affected by the strong energetic interactions among segments. In this region of $J(t)$ with compliance comparable to that of the glass state, the dynamic process is much related to the glass transition of the polymer. It is often referred to as the glassy relaxation. In the case of polystyrene, it has been shown by Plazek[19,20] that as the temperature is close to the glass transition temperature— below ~120 °C—the time-scale shift factors of the $J(t)$ curves with temperature in the softening (glass−rubber) region become greater than in the rubberlike-to-fluid region. As the viscosity is dominated by the terminal relaxation process, such an effect was also demonstrated by the divergence of the temperature dependences of the viscosity and recoverable compliance $J_r(t)$ as the temperature decreases below 120 °C. This difference in temperature dependence means that the principle of thermorheological simplicity breaks down between the rubberlike-to-fluid region and the glass−rubber region in this low-temperature range. As will be shown in this paper (see Figure 5), the rubber region in $J(t)$ is under the influence of the glassy relaxation; the thermorheological complexity actually occurs between the glassy-relaxation process and the processes in the rubber-to-fluid region instead of between glass−rubber region and the rubberlike-to-fluid region (see the note in ref 9 for explanations for the term "rubber(like)" used in this paper, which is related to this effect). The thermorheological complexity phenomenon not only is interesting but also should be important for our understanding of the glass transition. Using the quantitative description of the rubber(like)-to-fluid region of $J(t)$ in terms of ERT as the reference, the glassy-relaxation process at different temperatures are characterized quantitatively and consistently in this study. In this way, the whole range of chain dynamics— covering motions corresponding to sub-nanoscales, the Rouse-segmental length (~2 nm), the entanglement distance (7.6 nm), and the length scale of the whole molecule ($\gtrsim14$ nm for sample A; $\gtrsim23$ nm for sample B)—is revealed. The results of analysis at different temperatures are displayed in the $G(t)$ form. Through the molecular picture of ERT, the basic mechanism for the thermorheological complexity is analyzed, and the relation between the thermorheological complexity and the glass transition is studied.

2. Calculation of Creep Compliance

The creep compliance is related to the relaxation modulus by the convolution integral:

$$t = \int_0^t J(t')G(t - t')\, dt' \qquad (3)$$

which originates from Boltzmann's superposition principle.[1] With $G(t)$ known, $J(t)$—the target function—can be calculated from eq 3. The convolution integral may be solved numerically by the method of Hopkins and Hamming,[22,23] which is detailed in Appendix A.

To incorporate the glassy-relaxation process into ERT, eq 2 is replaced by the following equation:

$$F(t) = 1 + \mu_A(t/\tau_A) + A_G \mu_G(t/\tau_G) \qquad (4)$$

where $\mu_G(t)$ represents the glassy-relaxation process and A_G is its relaxation strength. In using eq 4, it is expected that $\mu_G(t)$ is a much faster process than the normal-mode processes in μ_A-(t); the fast local segmental motions in $\mu_G(t)$ can be regarded as the sources of the random fluctuation forces in the Langevin equation from which $\mu_A(t)$ is derived.[5,8,24,25] As shown below, this is true except when the temperature is basically at the glass transition temperature, where the loss of effective ergodicity is expected to occur; therefore, the applicability of the Langevin equation should be questioned. The number of normal modes $N_e - 1$ in the $\mu_A(t)$ process is set to be 15 corresponding to the mass of a Rouse segment (m) being about 850^{10-18} and the entanglement molecular weight $M_e = 13\,500$.[2,4,5]

In this study, it has been found that the glassy-relaxation process can be well described by the Kohlrausch, Williams, and Watts (KWW) or stretched exponential form:

$$\mu_G(t/\tau_G) = \exp[-(t/\tau_G)^\beta] \quad 0 < \beta \le 1 \qquad (5)$$

For a relaxation process as given by eq 5, the average relaxation time is defined by

$$\langle \tau \rangle_G = \int_0^\infty \mu_G(t/\tau_G)\, dt = \frac{\tau_G}{\beta}\Gamma(1/\beta) \qquad (6)$$

where Γ is the gamma function. In the whole relaxation-time distribution, the glassy-relaxation region is situated in a certain position relative to the rubber-to-fluid region, where all the relaxation times are proportional to the frictional factor K.[26] We may express the relative position by

$$\langle \tau \rangle_G = sK \qquad (7)$$

where s is a proportional constant and has the unit of Da^2. Although s is not unitless, it can be regarded as a "normalized" glassy-relaxation time, as it represents the glassy-relaxation time with K fixed at 1 or any constant. In the neighborhood of T_g, the parameter s increases with decreasing temperature, reflecting the thermorheological complexity between the glassy-relaxation region and the rubber-to-fluid region.

As shown below (section 3.1), the line shape of $J(t)$ in the rubber(like)-to-fluid region is well described by ERT as expected, allowing the K value to be determined. The whole $J(t)$ curve can be calculated with A_g, β, and s as contained in eqs 4−7 as the adjustable parameters for fitting to the line shape in the short-time/small-compliance region ($< \sim 5 \times 10^{-7}$ cm²/dyn) of the measured $J(t)$. In the initial stage, we are mainly concerned with the line shape of $J(t)$; in the fitting process, we calculate the whole $J(t)$ curve at some fixed K value and allow it to shift along the time coordinate to fit to the $J(t)$ result measured at a certain temperature. After good fitting over the whole time range of $J(t)$ has been obtained, the absolute value of K for the temperature can be calculated from the shift factor.

Different parts of $J(t)$ in the small-compliance region are sensitive to these individual parameters in greatly different degrees. Specifically, with a properly chosen A_G value that will give the observed glassy compliance, $J_g = \lim_{t \to 0} J(t) \sim 10^{-10}$ cm²/dyn, β affects the $J(t)$ line shape virtually only in the small-compliance region, $< 10^{-8}$ cm²/dyn. The region $10^{-8} \sim 5 \times 10^{-7}$ cm²/dyn, while being insensitive to a change in β, is determined by the product of A_G and $\langle \tau \rangle_G$ or A_G and s with K being fixed; in other words, it is directly related to the integration area of $A_G \mu_G(t)$. Since A_G is very much dictated by the J_g value of the studied sample and can be easily quantified, the position in time of the glassy-relaxation region relative to the rubber-(like)-to-fluid region can be used to determine the s value. Under the condition that a particular measured curve (at a certain temperature of measurement) and the calculated curve are matched, while the shifting factor along the time coordinate obtained from the matching allows the K value to be calculated, the s value can be determined uniquely by monitoring the agreement between the calculated and measured curves in the β-insensitive region, $10^{-8} \sim 5 \times 10^{-7}$ cm²/dyn. With the s value determined this way, the β value can then be determined by comparing the calculated curve with the measured in the small-compliance region, $< 10^{-8}$ cm²/dyn. Following the above-described procedure, a set of the parameters: A_G, β, and s can be uniquely determined for the system at a certain temperature. While A_G and β are very much independent of temperature, s increases significantly with decreasing temperature. The approach to the $J(t)$ line-shape analysis will be further illustrated in Figure 3 with an actual example described below.

### 3. Comparison with Experimental Results

3.1. Creep Compliance Curves. Plazek has reported the creep compliance results of two nearly monodisperse polystyrene samples in the entanglement region,[19,20] denoted by A and B here: A with $M_w = 4.69 \times 10^4$ and B with $M_w = 1.22 \times 10^5$. Even though the samples are nearly monodisperse, eq 1 needs to be convoluted with their molecular weight distributions to calculate $G(t)$ and then $J(t)$ for comparison with experimental results. The convolution only affects the rubberlike-to-fluid region. As shown previously,[2−5] the Schulz distribution[27] should be a good representation of molecular-weight distribution for samples such as A and B. The polydispersity of the Schulz distribution is characterized by the single parameter Z ($M_w/M_n = (Z + 1)/Z$). In the present analysis of $J(t)$, Z is used as an adjustable parameter. Close agreements between the calculated and measured $J(t)$ curves have been obtained with $Z = 20$ for both samples, corresponding to $M_w/M_n = 1.05$.

From the analyses of the $G(t)$ curves of a series of polystyrene samples of different molecular weights, with $M_e = 13\,500$ calculated from the plateau modulus $G_N = 2 \times 10^6$ dyn/cm², the frictional factor K is found to be independent of molecular weight to as low as just above M_e and is determined to be 4.7 $\times 10^{-9}$ within a small experimental error at 127.5 °C (see Table 1).[2,5] As shown in Figures 1 and 2, the $J(t)$ curves of samples A and B measured at different temperatures are compared with the curves calculated, through eq 3, from the $G(t)$ calculated using eqs 1 and 4−7 with $K = 5 \times 10^{-9}$ and $G_N = 2 \times 10^6/1.057$. The factor 1.057 in the G_N value used is the ratio of the product of density ρ and absolute temperature T between 127.5 and 100 °C. It is used here for conveniently comparing the calculated $J(t)$ curves with Plazek's results, which have all been reduced along the compliance axis by the factor $\rho T/\rho_o T_o$ using 100 °C as the reference point (see Figure 1 of ref 19 and Figure 7 of ref 20). Thus, Figures 1 and 2 use a mixed reference

TABLE 1: Frictional Factor K from $G(t)$, $J(t)$, Viscosity and Diffusion Results

	from $G(t)$	from $J(t)$[b]	from viscosity[c]				from diffusion[d]	
	series of samples[a] $3.4 \times 10^4 \leq M_w$ $\leq 1.1 \times 10^5$	$M_w = 4.69 \times 10^4$	$M_w = 9.4 \times 10^4$	$M_w = 1.89 \times 10^5$	$M_w = 6.0 \times 10^5$			average[e]
$K(127.5\ ^\circ\text{C}) \times 10^9$	$4.7 \pm 8\%$	4.8	5.7	4.9	5.8		$(5.7)^f$	$5.2 \pm 10\%$
$K(174\ ^\circ\text{C}) \times 10^{12}$	$(2.1)^f$	$(2.1)^f$	2.6	2.0	2.0		2.5	$2.3 \pm 14\%$

[a] Ref 2. [b] This study. [c] Ref 29. [d] Refs 33−35. [e] The average values are obtained from averaging over the values not enclosed in parentheses. [f] Values in parentheses are calculated from the shown values at the other temperature using the ratio between the two average K values.
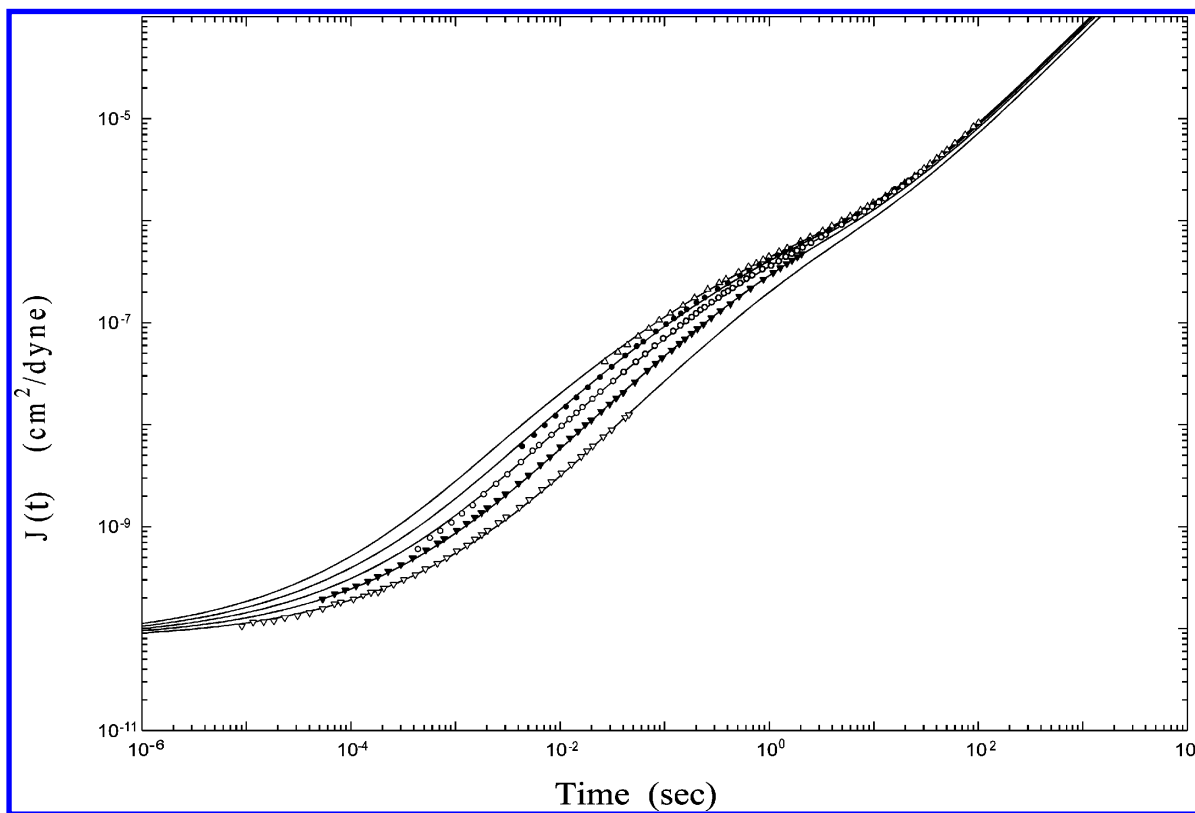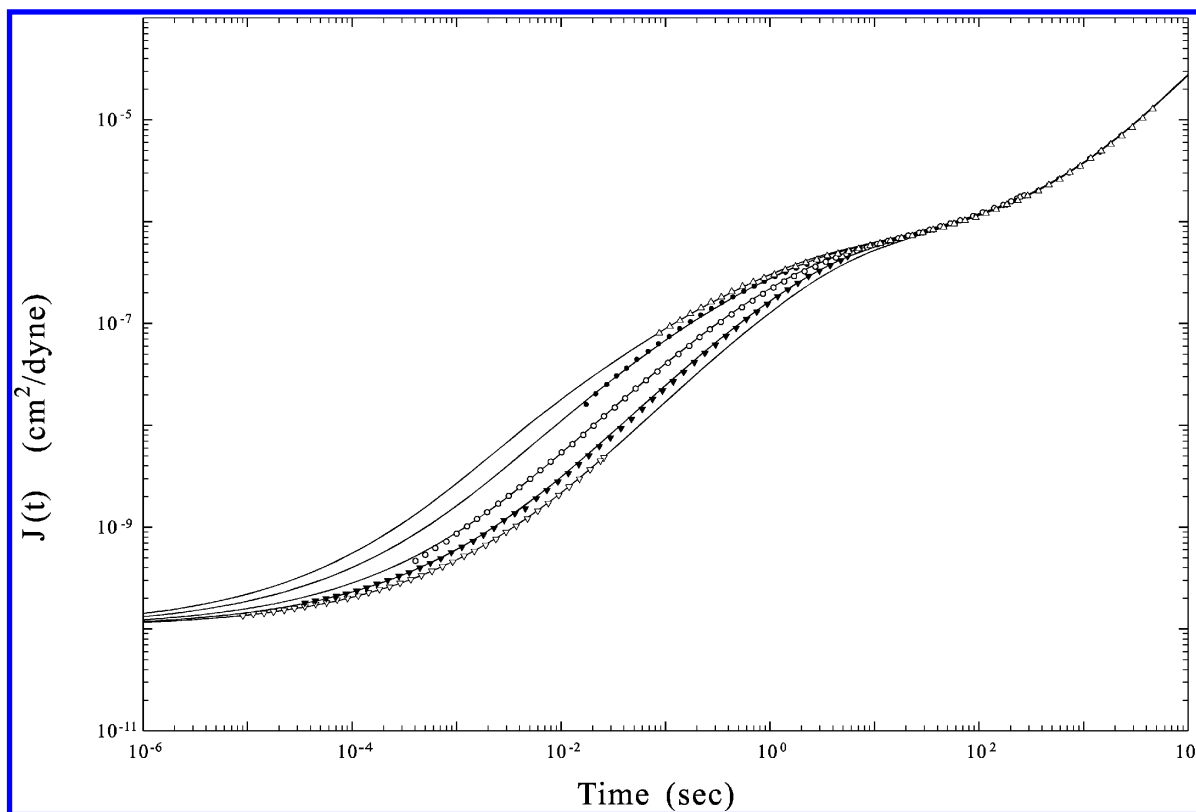

Figure 1. Creep compliance $J(t)$ data of sample A measured at 114.5 ($\triangle$); 109.6 ($\bullet$); 104.5 ($\bigcirc$); 100.6 ($\blacktriangledown$); and 97 ($\triangledown$) °C in comparison with the theoretical curves (—; from left to right, respectively) calculated with $K = 5 \times 10^{-9}$, $G_N = 1.89 \times 10^6$ dyn/cm^2; and the A_G, β, and s values as explained and given in the text.

system: 100 °C as the reference temperature for the compliance coordinate and 127.5 ± 0.4 °C for the time coordinate.[28,29] The shown fittings between the calculated and measured $J(t)$ curves are done by visual superposition with the aid of a graphical software.[30] Being wavy, each $J(t)$ curve has three bending points: two concaves and one convex as shown in the figures. Because each bending point basically denotes a position in the two-dimensional plot of log $J(t)$ versus log t, the matching between the calculated and measured curves around each bending point allows one to determine the absolute value of compliance (reduced to 100 °C and thus is independent of temperature) and the relative value of time (dependent on temperature). And the simultaneous matching over two bending points is a key criterion for determining the line shape of $J(t)$. In the shown close agreements between the calculated and measured $J(t)$ curves, for sample A no shift along the J axis is required for all the curves; for sample B no shift along the J axis is required at 105.5, 101.0, and 98.3 °C, while a shift of the experimental data upward by ∼5% is made (for a slightly better agreement than can be achieved without making such a shift) at 119.8 and 113.8 °C. All the agreements in line shapes as shown in Figures 1 and 2 involve two bending points except at the lowest temperatures: 97 °C for samples A and 98.3 °C

for sample B. At these two lowest temperatures, since the parameters A_G and β are well-determined by the good fittings at other temperatures, the s values determined from the close agreements between the calculated and measured in the very low-compliance region, even though around only a single bending point, should be dependable as well. This is confirmed in the companion paper[31] and by the consistency between the composition of the $J(t)$ curves as shown in Figure 1 and that shown in Figure 2 of ref 19.[32] (See the note at ref 32.)

For all the calculated curves in close agreements with the measured results as shown in Figures 1 and 2, the A_G values are 5482 and 4119 giving $J_g = 7.69 \times 10^{-11}$ and 1.02×10^{-10} cm^2/dyn for samples A and B, respectively, while $\beta = 0.41$ for both samples. The difference in A_G between samples A and B is directly related to their difference in J_g, which is quite apparent by a visual examination of the experimental results. The larger J_g of sample B should be due to the presence of residual plasticizers which was regarded by Plazek[20] as the cause for its smaller values and weaker temperature dependence of viscosity at temperatures close to T_g in comparison with a normal polystyrene sample of comparable molecular weight (see Figure 11 of ref 20). This association is further confirmed by the smaller frictional factors extracted from the $J(t)$ line-shape analysis for

Figure 2. Creep compliance $J(t)$ data of sample B measured at 119.8 ($\triangle$); 113.8 ($\bullet$); 105.5 ($\circ$); 101.0 ($\blacktriangledown$); and 98.3 ($\triangledown$) °C in comparison with the theoretical curves (—; from left to right, respectively) calculated with $K = 5 \times 10^{-9}$, $G_N = 1.89 \times 10^6$ dyn/cm²; and the A_G, β, and s values as explained and given in the text.

sample B as shown in the next section. Because the plasticizer molecules are very mobile, their presence in sample B will cause a fast relaxation process of very small relaxation strength to occur in $G(t)$, and in effect gives rise to some additional free volume Thus, the residual plasticizers in sample B have the effect of reducing somewhat the glassy compliance—as clearly visible in the $J(t)$ results of Plazek—as well as the value of the frictional factor K. However, the entanglement molecular weight is virtually not affected at all because there is only a residual amount of the plasticizer. As a result, the interrelations (ratios) among the relaxation times τ_A, τ_X, τ_B, and τ_C, which are determined only by the structural factors—functions of the normalized molecular weight M/M_e—are not affected;[2−5,8] in other words, the line shape of the viscoelastic spectrum over the rubber-to-fluid region will not be affected. As A_G is reduced by about 25% by the residual mobile plasticizer molecules, the glassy-relaxation region in sample B will be directly affected. However, as the discrepancy is only 25%, some of the information obtained from the $J(t)$ line-shape analysis of sample B can still be used; clearly the K value obtained from sample B cannot be used. This will be further discussed below over the results obtained from analyzing the $J(t)$ data.

In Figure 3, we compare three $J(t)$ curves calculated at three different β values: 0.36, 0.41, and 0.46 with $A_G = 5482$ and $s = 56550$ obtained for sample A at 97 °C; the one with $\beta = 0.41$ is the calculated curve shown in Figure 1 for sample A at 97 °C. The comparison illustrates the independence of $J(t)$ in the region $10^{-8} \sim 5 \times 10^{-7}$ cm²/dyn from the variation in β as described in the previous section. At the same time, the comparison also illustrates the sensitivity of the $J(t)$ line shape in the small-compliance region ($<10^{-8}$ cm²/dyn) to the change in β. From comparing the differences among the three curves calculated at different β values and the close agreement between the calculated curve ($\beta = 0.41$) and the experimental points

shown in Figure 1, the uncertainty of the β value determined to be 0.41 should be well within ±0.02.

3.2. Frictional Factor, K. For sample A, the frictional factor K at 127.5 °C can be first calculated from the time-scale shift factor obtained from superposing the calculated $J(t)$ curve on that measured at 125 °C as described in section 2 and then corrected for the temperature difference between 127.5 and 125 °C using the temperature dependence of its viscosity.[19,29] In this way, $K = 4.8 \times 10^{-9}$ is obtained in quantitative agreement with those determined from the analyses of the $G(t)$ results as reported before and mentioned above as well as those calculated from the viscosity[29] and diffusion[33−35] data. The agreement of the K values as shown in Table 1 (see Appendix B as well) is rigorous and significant, considering the constancy of K over a wide range of molecular weight and that these K values are obtained from analyzing experimental results measured independently by totally different kinds of instruments—strain-controlled versus stress-controlled rheometer—and of quantities of different nature—viscoelasticity versus diffusion.

For sample B, the frictional factor at 127.5 °C can be calculated first from the time-scale shift factor obtained from the superposition of the calculated with the $J(t)$ curve measured at 134.5 °C or at 119.8 °C and then corrected for the temperature difference using the temperature dependence of the viscosity of a normal (uncontaminated) polystyrene sample with a comparable molecular weight.[29] We obtain $K = 3.7 \times 10^{-9}$ if through 134.5 °C and $K = 3.0 \times 10^{-9}$ if through 119.8 °C. Both these two values are somewhat smaller than that for a normal sample, particularly the latter, supporting the presence of residual plasticizers in sample B. Furthermore, the presence of residual plasticizers in sample B has a larger effect, as in comparison with a normal sample, on its viscosity or frictional factor at a temperature close to T_g than at a higher temperature. This is the reason, to which Plazek attributed the smaller values
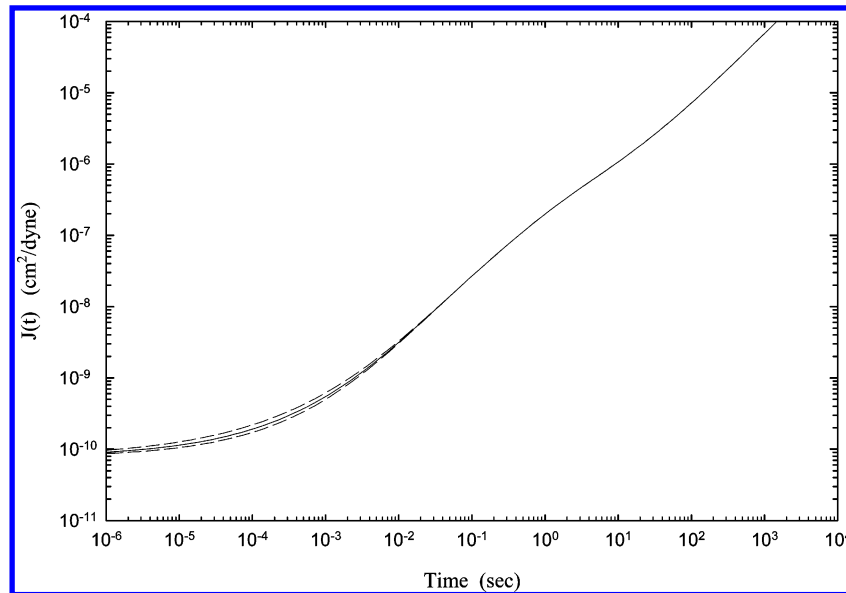
Figure 3. Comparison of the $J(t)$ curves calculated at $\beta = 0.36$ (upper dashed line), 0.41 (solid line), and 0.46 (lower dashed line) with $A_G = 5482$, $s = 56550$; the one with $\beta = 0.41$ is the same as the calculated curve shown in Figure 1 for sample A at 97 °C.
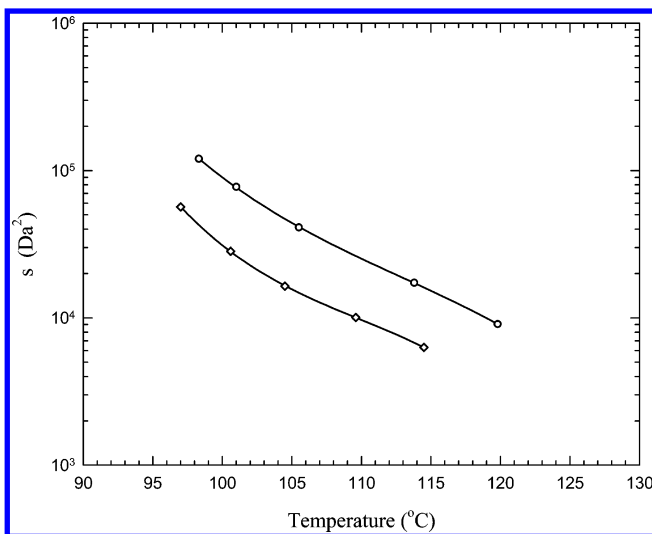
Figure 4. Normalized glassy-relaxation time s of samples A ($\diamond$) and B ($\bigcirc$) at different temperatures. See the text.

and weaker temperature dependence of the viscosity of sample B in the temperature region close to T_g.[20] This is clearly also reflected by the smaller K value of sample B obtained through 119.8 °C than through 134.5 °C.

Due to the presence of residual plasticizers in sample B, the K values obtained from sample B cannot be included in Table 1, which shows the molecular weight independence of K. In the companion paper,[31] the obtained K values for sample A from 127.5 to 97 °C are listed in Table 1; the consistency between the temperature dependence of K and that of viscosity (as $\eta/\rho T$) is shown in Figure 5.

3.3. Thermorheological Complexity. The thermorheological complexity as first pointed out by Plazek[19,20,36] in reporting his $J(t)$ results is shown caused by the increase of the normalized glassy-relaxation time s with decreasing temperature. The s values that give the close fittings between the theory and experiments as shown in Figures 1 and 2 are shown as a function of temperature for both samples together in Figure 4. These two molecular-weight dependence curves of s are parallel with each other indicating a similar effect taking place in both the systems. Over the shown temperature range, s increases by about

an order of magnitude with decreasing temperature. One can basically superpose the curve of sample A onto that of sample B by multiplying the s values of sample A by a factor of 2.6.

While the frictional factor K in the $\mu_X(t)$, $\mu_B(t)$, and $\mu_C(t)$ processes is independent of molecular weight to as low as just above M_e (see Appendix B), the frictional factor in the $\mu_A(t)$ process denoted by K' has been found to have a plateau value $\sim 3.3K$ in the high molecular-weight region, start to decline at $M/M_e \sim 10$ with decreasing molecular weight, and become identical to K as $M/M_e \rightarrow 1$.[2,5] The same molecular-weight dependence of K/K' is also observed for the blend-solution system[4,5] when it is expressed in terms of the normalized molecular weight: M/M_e for the pure melt and M/M_e' for the blend solution ($M_e' = M_e W^{-1}$ where W is the weight fraction of the entangled component; see the note at ref 37).[37] The dependence of K'/K on M/M_e (or M/M_e') can be described by the empirical equation:[4,5]

$$\frac{K'}{K} = \frac{2.525}{\exp\left[-0.643\left(\dfrac{M}{M_e} - 4.567\right)\right] + 1} + 0.769 \quad (8)$$

The dependence of K'/K on M/M_e has been explained as due to the free volume at chain ends being always available to the modes of motion along the primitive path while $\mu_A(t)$ is affected by the free volume around each entanglement strand, which depends on the molecular weight of the bulk.[2,5] As calculated from eq 8, $K' = 1.61K$ for sample A; $K' = 3.16K$ for sample B. These two K' values differ by a factor of 1.96. This ratio is close to that between the s values obtained for samples A and B at the same temperature. Since the product of A_G and s is what matters in determining the s value as explained in section 2, the difference between 2.6 and 1.96 is most likely related to the A_G value for B being somewhat smaller that that for A. Indeed, the product of 5482 (A_G of sample A) and 1.96—the expected normal situation—is very close to that of 4119 (A_G of sample B) and 2.6—the situation disturbed by the presence of residual plasticizers. The presence of residual plasticizers affects the line shape in the glassy-relaxation process region of sample B somewhat. As the distortion of the $A_G\mu_G(t)$ line shape is not large, the comparison of the two sets of results can still reveal that the dynamics of the whole $\mu_G(t) - \mu_A(t)$ region—not limited

to the $\mu_A(t)$ process—are characterized by relaxation times depending on molecular weight in the same way as K' (or K'/K as given by eq 8). This will be more clearly illustrated below (section 4.2) in the comparison the $G(t)$ line shapes in the glassy-relaxation region between samples A and B.

3.4. Fitting Parameters. It is advisable at this point to summarize the parameters involved in the theoretical fitting to the $J(t)$ line shapes of samples A and B as described above and discuss their uniqueness and significance. The relevant parameters involved in describing the $J(t)$ line shapes over eight decades in time in one case and over nine decades in the other case are A_G, β, s (or either τ_G or $\langle\tau\rangle_G$), M_e, K, K' (or K'/K), Z, and m. Among these parameters, most have been predetermined.

The entanglement molecular weight M_e has been determined independently from the plateau modulus—a static property. An error in the M_e value will lead to an error in the obtained K value because both M_e and K appear in the equations for the relaxation times τ_A, τ_X, τ_B, and τ_C; thus, an accurate determination of M_e is essential. $M_e = 13\,500$ has been obtained from the convergence of the assumed M_e value in consistence with the plateau modulus value obtained in the least-squares fitting process of the quantitative $G(t)$ line-shape analysis.[2,4,5] This M_e value is also confirmed by the close agreement with the value 13 300 determined by the integration method.[38]

With the accurately determined M_e, the frictional factor K was found independent of molecular weight from an extensive $G(t)$ line-shape analysis. In the $G(t)$ line-shape analysis, the polydispersity of the studied nearly monodisperse samples need be considered. The polydispersity parameter Z values obtained from the $G(t)$ line-shape analyses are extremely well-behaved; they fall between $Z = 30$ and 120 corresponding to $M_w/M_n = 1.03\sim1.01$, well within the range expected for a nearly monodisperse sample. The Z parameter affects mainly only the *shape* of the $G(t)$ curve in the terminal region; any possible small uncertainty in Z virtually has no effect on the obtained K value. Thus, the obtained molecular-weight independence of K is virtually not affected by the polydispersity variation among the studied nearly monodisperse samples.

The dependence of the K'/K ratio on molecular weight as phenomenologically described by eq 8 was determined from the relative position of the $\mu_A(t)$ process region to the plateau-terminal region by the $G(t)$ line-shape analyses.[2,4,5]

The molecular weight (m) of a Rouse segment, which determines the number of normal modes in $\mu_A(t)$, mainly affects the interface region between the energetic interactions-derived dynamic process ($A_G\mu_G(t)$) and the entropy-derived dynamic processes (the ERT processes: $\mu_A(t)$, $\mu_X(t)$, $\mu_B(t)$, and $\mu_C(t)$). The $A_G\mu_G(t)$ process and the ERT processes are of different nature; thus, a discontinuity occurring at the interface between the two intrinsically different kinds of dynamic processes is not surprising. Using eqs 1, 4, and 5 for the line-shape analysis, we have substituted a discontinuity for a somewhat smoother transition as should most likely occur in reality. The discontinuity picture can be considered as a first-order approximation and should work well if the location of discontinuity as represented by the m value is properly chosen. $m = 850$ falls within the range of the values determined by various techniques[10–18] with small variations. The discontinuity approximation and the proper choice of m are supported by the extensive close agreements between the calculated and measured $J(t)$ curves as shown in Figures 1 and 2.

The facts that the K value obtained for sample A at 127.5 °C agrees closely with the values obtained previously (see Table 1) and that the obtained Z value (= 20; corresponding to $M_w/$

$M_n = 1.05$) is well within the expected range allow us, to the same effect, to regard K and Z along with M_e, K' (or K'/K as given by eq 8), and m as predetermined parameters. In other words, A_G, β, and s are the main fitting variables in this study, affecting the small-time/small-compliance region of $J(t)$. The end result is the seamless quantitative description of $J(t)$ over the whole time range. Here, it should be stressed that the foundation for the quantitative description of $J(t)$ is ultimately K being independent of molecular weight. Because of the success of ERT as represented by the molecular-weight independence of K, theoretically, there is no limit to the time range of $J(t)$ that can be analyzed, depending on the molecular weight of the sample under study.

Among the three variables A_G, β, and s, as indicated above, A_G is basically dictated by the glassy modulus—the reciprocal of the glassy compliance J_G—and β is only sensitive to the $J(t)$ line shape in the small-compliance region, $<10^{-8}\,\mathrm{cm^2/dyn}$. Thus, the determination of the best values for A_G and β is effectively decoupled from that of s, which reflects the shift with temperature of the $J(t)$ curve in the $10^{-8} \sim 5 \times 10^{-7}\,\mathrm{cm^2/dyn}$ region along the normalized time coordinate. (In this study, the time coordinate under a fixed K value, as chosen to be 5×10^{-9} in Figures 1 and 2, is regarded as a normalized time coordinate.) The whole thermorheological complexity in $J(t)$ is reduced to the simple change in s with temperature shown in Figure 4. This reduction is of particular significance as we can notice in Figures 1 and 2 that the shift with temperature in the $\sim5 \times 10^{-7}\,\mathrm{cm^2/dyn}$ region is not as large as that in the $\sim10^{-8}\,\mathrm{cm^2/dyn}$ region. The thermorheological complexity in $J(t)$, even though being temporally uneven, is fully explained by the simple change in s, which, very importantly, has a clear physical meaning—namely, representing the stronger temperature dependence of the energetic interactions-derived dynamic process than that of the entropy-derived ones. How the temporal unevenness of the thermorheological complexity can arise from the simple change in s will be explained in section 4.1.

Thus, although on the surface there are eight parameters involved in calculating the $J(t)$ curves in quantitative agreement with the measured ones over the whole time range, the whole thermorheological complexity in $J(t)$ is uniquely represented by the simple change in s with temperature as all the other parameters can be determined independently beforehand or from the $J(t)$ line-shape analysis in a specific region.

It is advisable here to comment on the large dynamic range revealed by the $J(t)$ line-shape analysis—6 decades—as shown in Figures 1 and 2, which should be rare, if ever been done. Two main reasons make this wide range of analysis possible: The first is the consistently accurate $J(t)$ data of Plazek over a wide dynamic range, covering four decades in a single creep run in the best cases. The second is the correctness of the ERT-based functional form used to analyze the $J(t)$ data; the close agreement between the calculated and measured guides the overlapping and correlation of the $J(t)$ data measured at different temperatures, which extends one decade of dynamic range (see the note in ref 32). Then, the theoretical equation allows the results of analysis to be extended for another decade in the flow region.

To put the combination of eqs 1, 4, and 5 in a proper perspective, it may be pointed out that while ERT is a molecular theory, the inclusion of $A_G\mu_G(t/\tau_G)$ as defined by eqs 4 and 5 is a phenomenological description. Using the stretched exponential form characterized by the three parameters A_G, β, and τ_G is a common practice in describing an observed dynamic process closely or directly related to the glassy-relaxation process of a
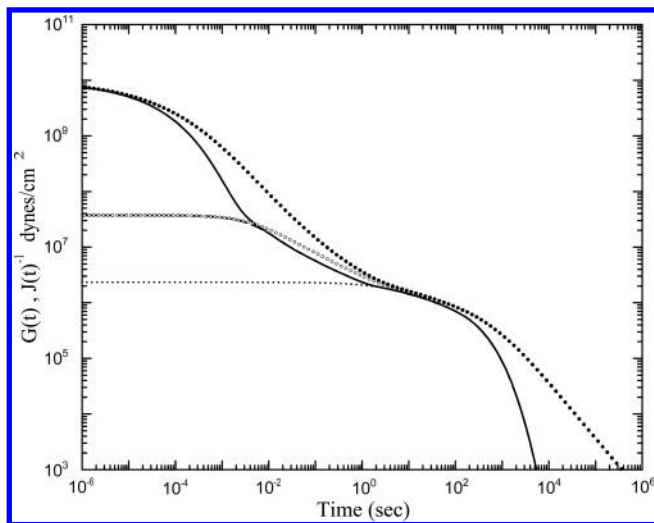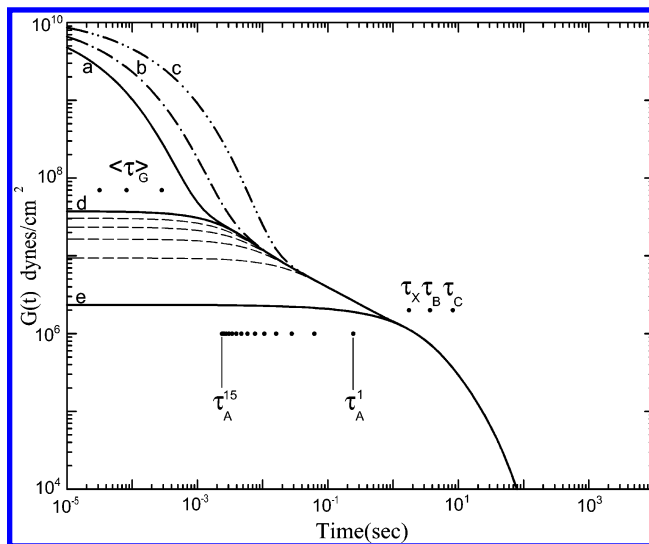
Figure 5. Comparison of the $G(t)$ (—) and $J(t)^{-1}$ (•••) curves for sample B at 113.8 °C (same $J(t)$ as the corresponding one shown in Figure 2). Also shown are the curves calculated without the $A_G\mu_G(t)$ process: (- - -) for $G(t)$ and (∘∘∘) for $J(t)^{-1}$; the dotted line indicates the $G(t)$ curve calculated without both $A_G\mu_G(t)$ and $\mu_A(t)$ processes.
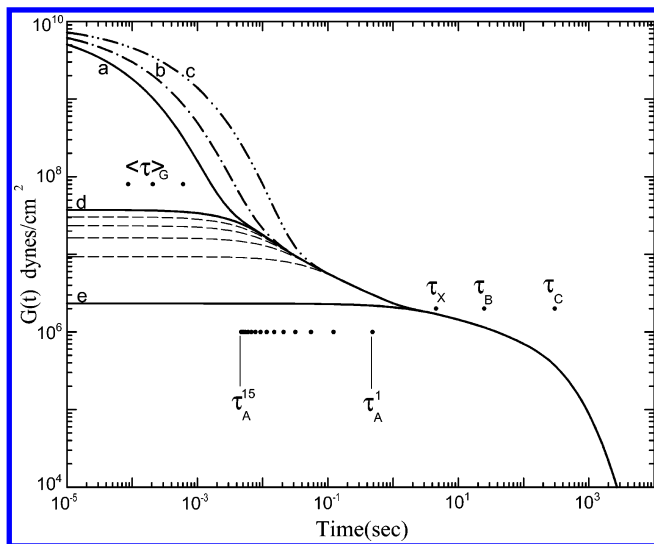

Figure 6. Calculated $G(t)$ curves corresponding to three $J(t)$ curves shown in Figure 1 for sample A: a, for 114.5 °C (—); b, for 104.5 °C (− · −); and c, for 97 °C (− ·· −). Line d is calculated without the $A_G\mu_G(t)$ process; line e is calculated without both the $A_G\mu_G(t)$ and $\mu_A(t)$ processes. The (- - -) lines from bottom up represent the sums of line e and the first 3, 6, 9, and 12 modes in $\mu_A(t)$, respectively. The dots represent the locations of the relaxation times as indicated. In the three dots under $\langle\tau\rangle_G$, the left one is for a; the middle one is for b; and the right one is for c.

glass-forming polymer or liquid[39,40] In fact, being described by a stretched-exponential form is considered as one of the canonical features of the T_g-related dynamic process. Even though it is generally understood that the three parameters (A_G, β, and τ_G) are closely related to the energetic interactions among the molecules or polymer segments, there is currently no molecular theory for relating them. Although we do not have the microscopic knowledge of the three parameters, from the results obtained from the $J(t)$ line-shape analysis, particularly the change in s with temperature, an informing *large picture* of the polymer dynamics can be revealed as discussed below.

4. Discussion

4.1. Comparison of $J(t)$ and $G(t)$. Shown in Figure 5 is the comparison of the curves of log $G(t)$ and log $J(t)^{-1}$ versus log t calculated with $K = 5 \times 10^{-9}$ at the s value corresponding to 113.8 °C for sample B. One can see that the $G(t)$ curve has clear line-shape features showing the separate processes as given in eqs 1 and 4, while the solution of the convolution integral (eq 3) for calculating $J(t)$ "smears" the separate features greatly. To illustrate this, both the $G(t)$ and $J(t)$ curves calculated without the contribution of the $A_G\mu_G(t)$ process are shown for comparison with the full curves. One can see that the influence of the $A_G\mu_G(t)$ contribution in $J(t)$ extends to the time region corresponding to the $\mu_A(t)$ process; in contrast, the $A_G\mu_G(t)$ and $\mu_A(t)$ processes in $G(t)$ are localized in the individual time regions where they occur and are well separated. Thus, the stronger temperature dependence of the $\mu_G(t)$ process can much affect $J(t)$ in the time region corresponding to the $\mu_A(t)$ process. In other words, in $J(t)$ the effect of the increase in s with decreasing temperature extends to the region around ~5 × 10^{-7} cm²/dyn instead of being only localized in the time region of the glassy relaxation $\mu_G(t)$. As the effect diminishes gradually with time scale, the temperature dependence in the region around ~5 × 10^{-7} cm²/dyn is not as strong as that in the glassy-relaxation region—this is the temporal unevenness of the thermorheological complexity in $J(t)$ as pointed out above. The unevenness has been first observed by Plazek[20] (see Figure 9 of ref 20) in saying "The divergence seen in the region of the 'knee' of the reduced (recoverable compliance) curve indicates that all of the retardation mechanisms do not have the same temperature dependence".

Indeed, this observation is an unusual discovery as Plazek stated "This discrepancy would not have been detected without a large range of time scale". However, without the help of a valid molecular theory as the base, this observed phenomenon has not been given a full explanation for more than 30 years. Here, we show that the intricacy arises mainly from the smearing effect of going through the convolution integral in eq 3 and that the source of the whole phenomenon is traced back to a rather simple physical effect.

For sample A, a similar comparison of the curves of log $G(t)$ and log $J(t)^{-1}$ versus log t as that shown in Figure 5 is observed as it should. In this case, the glassy-relaxation process has a small yet basically negligible effect on the flow region of $J(t)$ as well because its terminal region is relatively not that far away due to its smaller molecular weight. The effect becomes more obvious as s becomes larger with decreasing temperature (see Figure 1).

4.2. Thermorheological Complexity as Displayed in $G(t)$. As shown in this study, despite the smearing effect in $J(t)$, the whole range of the $J(t)$ curves can be analyzed in the framework of ERT into which $A_G\mu_G(t/J_G)$ is incorporated, revealing the dynamics in different time regions. Using the results obtained from the analysis of $J(t)$, the hierarchy of the dynamic processes can be displayed in the $G(t)$ form for a clearer discussion. In Figures 6 and 7, we show the $G(t)$ curves calculated with $K = 5 \times 10^{-9}$ for samples A and B, respectively, at the s values corresponding to 114.5, 104.5. and 97 °C for A and 113.8, 105.5. and 98.3 °C for B. In these figures, the curves calculated without the contributions of $A_G\mu_G(t)$ and without both of $A_G\mu_G(t)$ and $\mu_A(t)$ are also shown. The differences between these curves correspond to the separate contributions of the $A_G\mu_G(t)$ and $\mu_A(t)$ processes. In these figures, the locations of the relaxation times, $\langle\tau\rangle_G$, τ_A^p (for the normal modes of $\mu_A(t)$; $p = 1, 2, ..., 15$), τ_X, τ_B, and τ_C are also indicated. The number of normal modes used for $\mu_A(t)$ (i.e., $N_e - 1 = 15$) is a very reasonable choice as it corresponds to the mass for a Rouse segment (m) to be about 850, which falls within the range of the values determined by

Figure 7. Calculated $G(t)$ curves corresponding to three $J(t)$ curves shown in Figure 2 for sample B: a, for 113.8 °C (—); b, for 105.5 °C (− · −); and c, for 98.3 °C (− ·· −). The rest are the same as in Figure 6.

various techniques with small variations.[10−18] Segmental motions within a chain section shorter than 850 is regarded as belonging to the glassy relaxation. The $\{\tau_A^p\}$ points as shown in Figures 6 and 7 indicate that the relaxation times of the high Rouse−Mooney modes are closely packed; thus in choosing the number of modes, to differ by one or two basically does not affect the main point that we shall make and discuss below.

τ_A^{15} is the relaxation time of the fastest among the modes that contribute to the modulus of entropy origin; it can be regarded basically as the motional time constant associated with a single Rouse segment τ_v. Thus, it is a key time constant for comparison with $\langle\tau\rangle_G$. As shown in Figures 6 and 7, the $\langle\tau\rangle_G$ values at the shown temperatures are all much shorter than τ_A^{15} for both samples A and B. The great disparity between $\langle\tau\rangle_G$ and τ_A^{15} appears basically consistent with the stochastic assumption in the Langevin equations, from which the theoretical expression of $\mu_A(t)$ is derived. At the highest shown temperatures (114.5 °C for A and 113.8 °C for B), the modulus due to $A_G\mu_G(t)$ has basically relaxed to a negligible level at $t = \tau_A^{15}$ ($G/R = 0.05$ and 0.12, respectively, where G is the glassy contribution, calculated from the $A_G\mu_G(t)$ term; and R is the rubbery contribution, the sum of the remaining terms). The validity of the Langevin equations should hold well here. At the intermediate temperatures (104.5 °C for A and 105.5 °C for B), the contributions arising from energetic interactions among segments and derived from entropy are of the same order of magnitude at $t = \tau_A^{15}$ ($G/R = 0.96$ and 1.3, respectively), indicating that the ergodic assumption behind the Langevin equations may become not totally valid. As the temperature decreases basically to the calorimetric T_g (at 97 °C for A and 98.3 °C for B), the contribution to the total modulus from the energetic interactions greatly exceeds the entropy-derived contribution at $t = \tau_A^{15}$ ($G/R = 11.7$ and 9.8, respectively), indicating vitrification at the Rouse-segmental level. At these low temperatures, the full validity of the Langevin equations should be questioned, even though $\langle\tau\rangle_G < \tau_A^{15}$. In this situation, the combination of the functional forms given for $A_G\mu_G(t)$ and $\mu_A(t)$ can be considered as a good phenomenological representation for the processes in the short-to-intermediate time region of $J(t)$. However, $\mu_A(t)$ can be regarded as what the Rouse−Mooney modes of motion would be if the glassy-relaxation process had not moved to

longer times in the normalized scale. Thus, what is shown at $\sim T_g$ in Figures 6 and 7 does not only tell us that at $t \sim \tau_A^{15}$ the rubbery elasticity has been overshadowed or basically replaced by the energetic interactions-based elasticity but also allows us to use the relaxation times of the various Rouse−Mooney modes as "graduations" of a yardstick for estimating the extent of the influence of the glassy-relaxation process.

In terms of $G(t)$, we can more directly illustrate the small distortion of the $A_G\mu_G(t/\tau_G)$ line shape by the residual plasticizers in sample B and further make it clear that the distortion does not really affect what can be revealed—namely, the ratio between samples A and B of the relaxation times in the whole $\mu_G(t)-\mu_A(t)$ region, not limited to the $\mu_A(t)$ process, follows that of K' (or K'/K as given by eq 8). The two sets of $G(t)$ curves as shown in Figures 6 and 7 have approximately the same one-to-one corresponding temperatures: 114.5 versus 113.8; 104.5 versus 105.5; and 97 versus 98.3. Both 97 and 98.3 are each close to the T_g of samples A and B, respectively.[41−43] The G/R ratios at the three corresponding temperatures being basically of the same magnitude: 0.05 versus 0.12; 0.96 versus 1.3, and 11.7 versus 9.88, clearly indicate that the dynamics of the whole $\mu_G(t)-\mu_A(t)$ region are characterized by relaxation times depending on molecular weight in the same way as K'. In fact, allowing for $\sim\pm25\%$ deviations between two corresponding curves, which can account for the difference in A_G between samples A and B as well as the small differences in temperatures, the two sets of $G(t)$ curves as shown in Figures 6 and 7 can basically superpose on each other in the whole $\mu_G(t)-\mu_A(t)$ region rather well with a shift factor of ~2 along the normalized time coordinate, expected from the ratio of K'/K between the two samples. In comparison with this factor, a 25% deviation is rather small; in other words, the above drawn conclusion is sound.

The separation of the energetic interactions-derived dynamic process $A_G\mu_G(t/\tau_G)$ and the entropy-derived ones with the former having a stronger temperature dependence as shown in Figures 6 and 7 is consistent with the separation of the glassy and rubbery components of the dynamic Young's modulus spectra by Inoue et al.[12,13] analyzing dynamic mechanical and birefringence results (see Figure 7 of ref 12). However, the spectra of the rubbery component of Inoue are limited to the $\mu_A(t)$ process region and the early part of the plateau region by the nature of their experiment. As shown in the companion paper,[31] the obtained temperature dependences of τ_A^{15} (equivalent to that of K) and $\langle\tau\rangle_G$ are respectively in close agreement with those of the viscosity and recoverable compliance obtained by Plazek.[19,29] At the same time, the temperature dependence of the rubbery component and that of the glassy component separated by Inoue et al. are shown to be in agreement, respectively, with those of the viscosity and recoverable compliance of Plazek in ref 13.

4.3. Comments Based on Literature Results of the Transition Zone. In general, it has often been indicated that the relaxation in the transition zone is independent of molecular weight.[1] However, this is based on the results obtained in the high molecular weight region where, as indicated by eq 8 for polystyrene, K'/K is independent of molecular weight (above $\sim10\ M_e$). In fact, the raw $J(t)$ data of Plazek show that at the same temperature sample B reaches the same compliance level in the small compliance region, say at 10^{-9} cm²/dyn, significantly later than sample A even though sample B is contaminated by residual plasticizers. The ratio between the two time values is estimated to be roughly that obtained above (~2) after their difference in K is taken into account (Note: Both Figures 6 and 7 are displayed under the same $K = 5 \times 10^{-9}$.) The similar

Whole Range of Chain Dynamics

J. Phys. Chem. B, Vol. 109, No. 37, 2005 **17663**

molecular-weight dependence of the transition zone (the $\mu_G(t)-$ $\mu_A(t)$ region) is also observed in other polymers. For instance, in the $J(t)$ results of poly(*cis*-isoprene) obtained by Nemoto et al.,[44] the transition region ($J(t)$ curve from $\lesssim 10^{-9}$ to $\gtrsim 10^{-8}$ cm²/ dyn; see Figure 1 of ref 44) of a sample with molecular weight at ~1.4 M_e occurs earlier by a factor of ~4.5 than those at higher molecular weights (>4 M_e),[45] which show very weak molecular-weight dependence. The similar effect also occurs in the $J(t)$ results of poly(vinyl acetate) obtained by Ninomiya and Ferry: [46] the transition region ($J(t)$ curve from $\gtrsim 10^{-9}$ to $\lesssim 10^{-7}$ cm²/ dyn) of a sample at ~1.5 M_e occurs earlier by a factor of ~2.5 than that in the high molecular-weight limit. All these results indicate that all the relaxation processes in the transition zone become faster significantly as the molecular weight is decreasing toward M_e. Except for polystyrene, there are not sufficient results to indicate clearly the onset and the magnitude of the molecular-weight dependence of the transition zone for different polymers. With the frictional factor K for polystyrene being independent of molecular weight as guidance for the universal behavior in the plateau-terminal region, the molecular-weight dependence in the transition zone should not be used directly as the basis for the iso-frictional correction in the study of the molecular-weight dependence of viscosity,[47] which is dominated by the K-determined long-time relaxation processes. Furthermore, as the temperature dependence in the glassy-relaxation region or the transition zone has been shown to be stronger, as in the polystyrene case under the present study, than in the rubber-to-fluid range for several different polymers,[36,48−51] the temperature dependence in the transition zone should not be used directly for correlating viscosity data measured at different temperatures when one of the involved temperatures is sufficiently close to T_g.[44]

4.4. Basic Mechanism for the Thermorheological Complexity. The process $A_G\mu_G(t)$ that describes the $J(t)$ curve in the small-compliance/short-time region is clearly derived from energetic interactions among segments. As shown above, the chain section of the Rouse-segment size is gradually stiffened by the energetic interactions with decreasing temperature until it is overwhelmed by the effect at ~T_g. Correspondingly, the increase in the parameter s with decreasing temperature suggests the existence of an additional dynamic time scale "normalized" with respect to K, which in turn suggests the existence of a corresponding structural length scale. Indeed, as s has the unit of Da², the mass size of the structure increases as $\propto s^{1/2}$ with temperature decreasing toward T_g. Clearly, such a structure has to be based on energetic interactions among segments. Based on what we have observed in the above analysis, this structure should have the following basic properties:

(1) The structure has a length scale and a lifetime, both of which increase with decreasing temperature. We can somewhat arbitrarily choose $G/R = 3$ as a criterion for designating the lifetime of the structure. $G/R = 3$ indicates a state which has relaxed considerably from $G/R \sim 10$—by a factor of $\sim e^{-1}$—which is about the value at $t = \tau_A^{15}$ when the temperature is at T_g; at the same time, the state is still much under the influence of the energetic interactions. Thus, the time when G/R reaches 3 can be regarded as a time constant that reflects the duration of the structure. Here, we simply refer to it as the lifetime of the structure and denote it by τ_S. From the calculations whose results are shown in Figures 6 and 7, one finds that for both the samples while $\tau_S < \tau_A^{15}$ at ~104.5−105.5 °C, τ_S has reached $\tau_A^6 - \tau_A^7$ at ~T_g. τ_A^p is the relaxation time of the mode of motion associated with a length scale $\sim (a^2/p)^{0.5}$ where a is the entanglement distance.[5,52] Thus, the size of the domain influenced by the

TABLE 2: Time Constants of Dynamic Processes in Sample A at Temperatures Close to T_g[a]

temp (°C)	with loss of ergodicity or non-ergodic		ergodic			
	$\langle\tau\rangle_G$ (s)	τ_S (s)	τ_A^1 (s)	τ_X (s)	τ_B (s)	τ_C (s)
104.5	.196	3.2 (3.53)[b]	587	4179	8798	19699
100.6	2.74	48.7 (49.4)[b]	4759	33779	71121	159232
97 $\approx T_g$	55.7	1193 (1002)[b]	48276	342661	721472	1615305

[a] Ergodic (entropy-derived) vs non-ergodic (or with loss of ergodicity; energetic interactions-derived). [b] Defined by $\tau_S = 18\langle\tau\rangle_G$; see ref 31.

energetic interactions increases as the temperature is lowered toward T_g. Of course, this is directly corresponding to the increase in the mass size of the structure ($\propto s^{1/2}$) as pointed out above. As defined above, the structural lifetime τ_S is of the order of $15-20\langle\tau\rangle_G$. And the length scale affected by the glassy-relaxation process or the length scale of the structure is ~3 nm (for $p = 6\sim7$; and $a = 7.6$ nm for polystyrene[5,38,53]) at ~T_g. Interestingly, this length-scale value is the same as that estimated for polystyrene from the calorimetric data based on an argument considering fluctuations in a "cooperatively rearranging region".[54,55] In general the length scales of glass-forming materials as obtained by different techniques are in the range 1~5 nm.[54−58] The crossing over τ_A^{15} by τ_S just before the temperature reaches T_g is a critical microscopic event for the eventual vitrification of the polymer material. In the companion paper,[31] for being able to reflect the temperature dependence of the glassy-relaxation process accurately and the effect on bulk mechanical property—by maintaining the same order of magnitude—the structural relaxation time is defined as $\tau_S = 18\langle\tau\rangle_G$ (see Table 2). The relative changes of these two kinds of characteristic times, $\tau_A^{15} = \tau_v$ and τ_S, with temperature in the case of sample A will be further studied.

(2) As induced by an applied strain, the stress on such a structure is developed on energetic interactions and relaxes as the interlocking of segments in the structure loosens up due to thermal motions. The structural lifetime is an important factor that needs to be included in the consideration of the diffusion constant associated with a Rouse segment (D) when the structure has a size greater than that of the Rouse segment as described above. Even when the length scale of the structure is greater than that of the Rouse segment, D can still be defined by the distance a Rouse segment has travelled statistically over a long period of time. This is clear as, in the rubberlike-to-fluid region, the $J(t)$ line shape remains unchanged with temperature;[59] the relaxation times τ_A^1, τ_X, τ_B, and τ_C, which are inversely proportional to D,[2,5−8] can be calculated from the K value obtained from the line-shape analysis as explained in section 3.2. In other words, as K can be determined—as listed in Table 1 of ref 31 for sample A from 127.5 to 97 °C—so D can be defined and obtained.

Based on the basic properties of the structure as described above, the thermorheological complexity between the glassy-relaxation region and the rubber-to-fluid region can be explained as in the following: Being Brownian motion, the diffusion constant of a Rouse segment can generally be expressed as

$$D = \frac{kT}{\zeta} \approx \frac{l^2}{\Delta t} \tag{9}$$

where l is the step length that the Rouse segment has moved in a time interval Δt. The only criterion for choosing Δt and l is that the steps are *independent* of one another; after a sufficiently

large number of steps of movement have taken place, the central limit theorem ensures that the dynamic process becomes Gaussian.[5,52] Here, we consider the time step Δt in a "normalized" scale by dividing it by K. The normalization has a similar sense as Figures 1, 2, 6, and 7 being displayed under a fixed K. As what will be discussed below has much to do with the fact that the normalized glassy-relaxation time s increases with decreasing temperature, it will be easier to explain the concepts in the normalized time scale. In the normalized scale, D is a constant—independent of temperature. When there is not the structure whose relaxation is described as above—as the situation expected to be at high temperatures—we can have a wide range down to very small values to choose l and Δt for satisfying eq 9. This is often referred to as the continuous (small-step) or "free" diffusion.[39,60] At a temperature close to T_g, the structure is formed with a certain lifetime τ_S (in the normalized scale), which increases as s increases; then the smallest independent time step that can be chosen is of the order of the lifetime of the structure $\Delta\tau \approx \tau_S \approx 15{\sim}20\langle\tau\rangle_G$ (all in the normalized scale). We can choose $\Delta\tau$ as the time step because $\Delta\tau$ is still much shorter than τ_A^1, τ_X, τ_B, and τ_C (all these time constants are constant in the normalized scale). Here, what has changed is that the diffusion regime has moved to longer times. Corresponding to $\Delta\tau$ being longer, a larger length scale d is expected for the step length; both $\Delta\tau$ and d increase with decreasing temperature. With $\Delta\tau$ and d chosen this way, the *normalized* diffusion constant can be kept constant as required:

$$DK \approx (d^2/\Delta\tau)K \approx (d^2/\tau_S)K \propto (d^2/\langle\tau\rangle_G)K = (d^2/s) = \text{const} \tag{10}$$

Because of the formation of the structure, the local segmental reorientation time directly related to the lifetime of the structure has lengthened greatly in the normalized time scale; however, the relaxation times (normalized) in the long-time region (τ_A^1, τ_X, τ_B, and τ_C) remain the same. In other words, in the real time (not normalized), the relaxation times in the long-time region are proportional to $K \propto \zeta/kT \approx \Delta\tau/d^2$ when the structure is formed, while the local structural relaxation time is proportional to $\langle\tau\rangle_G \propto \Delta\tau$. The temperature dependence of $\Delta\tau$ is expected to be stronger than that of $\Delta\tau/d^2$. This difference in temperature dependence is the basic mechanism for the thermorheological complexity as indicated by the analyses of the $J(t)$ curves at different temperatures in this study.

To satisfy the conditions for choosing $\Delta\tau$ and d, a likely dynamic process for the Rouse segment to take is by cooperative large-step jumping involving more than one Rouse segment. The cooperative large-step jumping has long been recognized based on the magnitude of the apparent activation energy near the glass transition.[39,61,62] Molecular dynamics simulations for glass-forming Lennard−Jones mixtures,[60,63] through the study of the van Hove self-correlation function, have clearly indicated the shifting of the diffusion regime to longer times as the temperature is lowered—similar to the effect as pointed out in the above analysis. Associated with this effect taking place is that the dynamics become not only spatially heterogeneous but also dynamically correlated; in other words, the dynamic process is no longer that described by continuous diffusion. Such dynamic heterogeneity and correlation have also been observed directly by confocal microscopy in the colloidal fluids near T_g.[64] Dynamic heterogeneity in glass-forming liquids and polymers in the vicinity of T_g has also been indicated by various studies using different techniques.[65−70] It is generally believed that dynamic heterogeneity implies the existence of a length scale, whose value at T_g—as much stimulated by the notion of the

cooperative rearranging regions (CRRs) of the Adam and Gibbs theory[71]—has been a subject of both theoretical and experimental studies.[54−58,72] Despite all the gained understandings, a precise relation between the length scale or CRRs and dynamic heterogeneity has still to be formulated. The time scale and the length scale involved in the above discussion of the thermorheological complexity are obtained from analyzing the bulk property $J(t)$; thus, they are macroscopically averaged values. How these values can be better defined at the molecular level should be most likely answered by comparing studies with various spectroscopies.

The viscoelastic behavior of polystyrene in approaching T_g as discussed above—namely, the discussion of $\langle\tau\rangle_G$ or τ_S versus τ_A^1, τ_X, τ_B, and τ_C—demonstrates what has been well-said by Sillescu[54] about a dynamically heterogeneous system: "..., a system may be heterogeneous and non-ergodic at times $t < 1$ s, but perfectly homogeneous and ergodic on a time scale of hours". To further illustrate this, we use the K and s values for sample A at temperatures close to T_g as listed in Table 1 of the companion paper[31] to calculate the non-ergodic and ergodic relaxation times for comparison, as shown in Table 2. In the relatively short yet macroscopic time scales of $\langle\tau\rangle_G$ or τ_S, the strong energetic interactions in forming the structure keeps many configurations from being explored, while in the long time scales of τ_A^1, τ_X, τ_B, and τ_C, there are enough time to explore the configurational space effectively, leading to entropy-derived modulus (as represented by the entropy force constant) and dynamics (as described by the Langevin equation). Below ${\sim}110$ °C, loss of ergodicity gradually takes effect in polystyrene.

The formation of an energetic interactions-based structure indicates that the glass transition is a thermodynamic phenomenon; at the same time, the structure having a lifetime indicates that it is also a dynamic phenomenon. The dual nature of the glass transition phenomenon has long been recognized experimentally. For a practical purpose, a T_g-related temperature is often determined by monitoring the occurrence of the glass−rubber relaxation by dynamic mechanical measurements fixed at a certain frequency as the temperature is varied.[1,73] Since both K and s change with temperature, so does the characteristic time of the glass−rubber relaxation in $G(t)$—often referred to as the α-relaxation time. Thus, the T_g-related temperature determined this way depends on the probing frequency. The traditional ways of defining the α-relaxation time will be compared with what will be obtained from the further analysis in the companion paper.[31] Another factor: nonequilibrium state at and below T_g makes the measured T_g depend on the cooling rate of the sample. Such an effect can be clearly observed in monitoring the specific volume as the temperature is lowered.[1,74] In this study, the nonequilibrium aspect of T_g is not a concern, as the systems under analysis should all be in the equilibrium state.[19] Either probing rate or cooling rate is an externally imposed condition. In this paper, we show that there is an intrinsic rate or time scale that plays a critically important role in the glass transition of a polymer, namely, the relaxation time of the highest Rouse−Mooney mode, τ_A^{15}. The crossing over τ_A^{15} by τ_S signals the start of vitrification at the Rouse-segmental level—the basic change at the molecular level corresponding to the transition of the bulk consistency from rubber to glass. Since the Rouse segment is the most basic structural unit in terms of which all the long-time viscoelastic behavior of the polymer can be described,[5] a fundamental change at the Rouse-segmental level—vitrification—is expected to have a dramatic effect on the bulk property. As the relative position of τ_S to τ_A^{15} is changed by the thermorheological-

Whole Range of Chain Dynamics

J. Phys. Chem. B, Vol. 109, No. 37, 2005 **17665**

complexity effect, the glass transition is closely related to the observed thermorheological complexity in $J(t)$. This topic will be further studied in the companion paper.[31]

Models have been proposed for the supercooled liquids involving the concept of domain,[39,40,71,75,76] all based on energetic interactions among particles or segments. A basic idea in all these is, either explicitly or implicitly, that the system moves from the region of free diffusion to one of "landscape"-(potential energy hypersurface) dominated dynamics as the temperature decreases toward T_g. Such a view is much supported by molecular dynamics simulations.[77,78] However, the thermorheological complexity—arising also from energetic interactions and related to the glass transition by the above-described mechanism—has never been considered in any of these models, as far as we know. The temperature dependence of K is usually described by the Fulcher and Tammann–Hesse (FTH) equation or the Williams–Landel–Ferry (WLF) equation.[1,79,80] The thermorheological complexity is more than the non-Arrehnius temperature dependence, which has been provided an explanation for or accepted in these models.

Similar to the phrase "vitrification at the Rouse-segmental level" used to represent the overwhelming of the entropy-derived modulus by the energetic interactions-derived contribution at the Rouse-segmental time scale $t = \tau_A^{15}$ as revealed above, Adachi and Hirano[51] proposed an idea of local vitrification based on their observation that below 230 K the ratio of the dielectric relaxation times of the normal and segmental modes in poly-(*cis*-isoprene) decreases with decreasing temperature. However, their physical picture is totally different; they attributed the weaker temperature dependence of the normal mode to the shortening of the effective normal-mode length scale caused by the vitrification taking place locally at some points distributed on the chain. They also reported that they did not observe the decrease in the relaxation strength $\Delta\epsilon$ and broadening of the distribution of the normal-mode relaxation times to support their picture. Although not really a direct indication of local vitrification as shown in the present analysis, their observation that the time–temperature superposition is not applicable over the whole frequency range as the temperature approaches T_g should arise from the same basic mechanism as for the thermorheological complexity in $J(t)$ of the polystyrene system under the present analysis. So is the stronger temperature dependence of the glassy component in comparison with that of the rubbery component as revealed by Inoue et al. analyzing the dynamic mechanical and birefringence results for several different polymers.[12,13,49,50] Thus, the thermorheological complexity is quite a general phenomenon; the existence of such an effect has been pointed out by the researchers in polymer rheology through the years without offering a fundamental explanation.[12,13,36,48–50] In this study, we show through the analysis and discussion of $\langle\tau\rangle_G$ or τ_S versus τ_A^1, τ_X, τ_B, and τ_C the mechanism behind it and its relation to the glass transition of a polymer.

The basic mechanism as proposed for the thermorheological complexity occurring in the polystyrene system should also be the reason for the breakdown of the Stoke–Einstein equation in relating the translational diffusion constant D_g with the shear viscosity η_s, which has been observed for glass-forming liquids, such as OTP (*o*-terphenyl)[81–83] and TNB (*tris*-naphthylbenzene),[84] when T_g is approached from above. Without the entropy-derived modes of motion as described by ERT in such liquids, $\eta_s \sim \int A_G \mu_G(t) \, dt$; similarly to what is explained above, $D_g \sim d^2/\Delta\tau$ while $\eta_s \sim \Delta\tau$. Thus, the diffusion constant is enhanced.

The only attempt ever made to explain the thermorheological complexity in polystyrene was by Ngai et al.[85] in terms of the so-called coupling model. The model is an explanation scheme based on the idea that the relaxation rate decreases with increasing time by scaling with an exponent $-n$ ($0 < n < 1$). They have made a link between n and the time-scale shift factor, in which the stretching parameter $\beta = 1 - n$. Regardless of whether their scheme is applicable in the glassy-relaxation region, it is hard to imagine that such a scheme would apply to the entropic region, which in the entangled case is described by ERT quantitatively over the whole range as shown in this study as well as previously[2–6,8] or which in the entanglement-free case by the Rouse theory.[3,5,86] It is shown that while, as expected from the molecular theories using the Rouse segment as the most basic structural unit, all the dynamic processes in the entropic region have the same time-scale shift factor, in the short-time region the energetic interactions-derived dynamic process, the glassy relaxation, has stronger temperature dependence. Such a simple physics also explains naturally in a precise way the temporal unevenness of the thermorheological complexity (section 4.1), which is clearly not within the scope of the scheme of Ngai et al. Furthermore, the coupling model does not give a physical picture, which would suggest that the thermorheological complexity and the breakdown of the Stoke–Einstein relation observed in glass-forming liquids arise from the same basic mechanism as the present analysis indicates.

5. Summary

Although the $J(t)$ results of Plazek of two nearly monodisperse polystyrene samples in the entanglement region were published more than 35 years ago, they remain basically unanalyzed, particularly in terms of a functional form which has a valid molecular theory as the basis. As a result, despite the extremely wide range of time they span, the rich information of polymer dynamics that they contain have remained basically untapped until this paper.

In this study, two classes of contributions to the relaxation modulus $G(t)$ are identified: One, $A_G\mu_G(t)$, originates from energetic interactions; the other, containing the four dynamic processes of ERT ($\mu_A(t)$, $\mu_X(t)$, $\mu_B(t)$, and $\mu_C(t)$) is derived from entropy. The relaxation functional forms of all the processes are given: phenomenological form for $A_G\mu_G(t)$; molecular expressions for $\mu_A(t)$, $\mu_X(t)$, $\mu_B(t)$, and $\mu_C(t)$. In terms of the $G(t)$ function, the $J(t)$ results of Plazek are successfully analyzed. We first show that the $J(t)$ results of the two nearly monodisperse polystyrene samples are well described by ERT in the rubber(like)-to-fluid region, giving the frictional factor K for the uncontaminated sample—sample A—in quantitative agreement with those obtained previously from analyzing the $G(t)$ results and calculated from the viscosity and diffusion data. This gives an confirmation—from an independent investigator and different type of measurement—to the validity of ERT. Then it is demonstrated that the successful description of $J(t)$ in the rubber(like)-to-fluid region in terms of ERT can be used as the reference frame, with respect to which the glassy-relaxation process that occurs in the small-compliance/short-time region of $J(t)$ can be analyzed meaningfully and profitably. The contributions from this study are manifold:

The unified quantitative analysis of the whole range of chain dynamics, from the glassy-relaxation region to the flow region, shows how the dynamic processes occur one after another as clearly displayed in the $G(t)$ form. Displaying the hierarchy of the dynamic processes in perspective, the analysis by itself has far-reaching application potential, for instance, for comparing

studies with other spectroscopies sensitive to dynamics at different length scales and for seeing how the hierarchy is affected if some structural modification is made to the polymer.

It is shown that in polystyrene the temperature dependence of the energetic interactions-derived glassy-relaxation process is stronger than that of the entropy-derived processes in the rubber-to-fluid region as the temperature is close to T_g, in agreement with the result obtained by Inoue et al.[12,13] The thermorheological complexity in $J(t)$ is shown arising from this difference in temperature dependence; the temporal unevenness in the observed complexity in $J(t)$ is revealed as due to the smearing effect of the convolution integral in eq 3.

Corresponding to the thermorheological complexity, the increase of the normalized glassy-relaxation time s with decreasing temperature indicates that a structure based on energetic interactions among segments occurs as the temperature is close to T_g. With decreasing temperature, both the length scale and lifetime of the structure increase; furthermore, the mass size of the structure is expected to increase as $\propto s^{1/2}$.

This study, making use of the molecular picture in ERT, gives microscopic information about the glass transition of polystyrene from a viewpoint that cannot be reached by the traditional approaches.[39] In fact, the entanglement effect has often been seen as an "obstacle"—by causing a viscosity increase of many orders of magnitude—to the study of the glass transition of a polymer when the convention of viscosity reaching 10^{13} poise[39,40] is to be used to indicate T_g. Here, because ERT enables the whole rubber(like)-to-fluid region in $J(t)$ to be analyzed, we turn entanglement to our advantage—namely, using the description of the rubber-to-fluid region as a reference frame for studying the glassy-relaxation process that occurs in the short-time region. Through the molecular picture of ERT, the following two important pieces of information related to the glass transition have been revealed:

(a) It is shown that for polystyrene the length scale of the energetic interactions-based structure is $\sim$3 nm at T_g in agreement with the value obtained from the calorimetric data.[54,55] Much to the credit of the notion represented by the 'cooperatively rearranging regions' of the Adam and Gibbs theory, the length scale at T_g has been the focus of various studies. This study represents a new methodology for studying it in an entangled polymer. As opposed to several techniques which require imposing external length scales to the studied material,[54-58] the yardstick for estimating the length scale in this study is provided internally (i.e., by the normal modes in the $\mu_A(t)$ process). This method has the advantage of being free of any surface effect, which may quite easily affect the result in the case that the material is studied in confined geometries; the surface effect is currently very much an issue of interpretation. In principle, the present method can be applied to any entangled polymer, as long as it is nearly monodisperse.[87,88] This would be particularly useful as the values of entanglement distance (a) of various polymers have been well documented.[5,38,53]

(b) It is shown that, corresponding to the rubber–glass transition of the polymer taking place at the calorimetric T_g, τ_S becomes greater than τ_A^{15} indicating vitrification at the Rouse-segmental level. Such a fundamental change at the Rouse-segmental level should be responsible for the dramatic change in the bulk mechanical property at $\sim T_g$. τ_S becoming greater than τ_A^{15} at $\sim T_g$ for a polymer suggests the question whether there is a physical time constant τ_1 that can be studied, characterizing the liquid state in a glass-forming liquid, which is to be surpassed by the structural (α-) relaxation time τ_S for

the glass transition to take place. So far such a time is set in an arbitrary way by the convention that τ_S reaches $100-1000$ s at $\sim T_g$.[39,54,89] The τ_S value at $\sim T_g$ shown in Table 2 is consistent with the convention.

It is shown that the basic mechanism for the thermorheological complexity deduced from the present study should be also responsible for the breakdown of the Stoke–Einstein relation observed in glass-forming liquids, such as OTP and TNB, near the glass–liquid transition. While the thermorheological complexity has been puzzling to polymer rheologists for years, the breakdown of the Stoke–Einstein relation has been actively studied in the past decade. The proposed mechanism allowing the two seemingly unrelated phenomena to be linked represents a new way to see and study the glass transition phenomenon.

Appendix A: Hopkins–Hamming Method for the Interconversion between $G(t)$ and $J(t)$

Equation 3 originates from Boltzmann's superposition principle and is a basic equation of linear viscoelasticity. $J(t)$ can be calculated numerically from $G(t)$ through eq 3 while $G(t)$ from $J(t)$ through the equivalent equation:

$$t = \int_0^t G(t')J(t - t')\,dt' \tag{11}$$

Here, we consider the case of $J(t)$—as the target function—from $G(t)$ using eq 3. In the Hopkins–Hamming method, the integration interval of eq 3 is divided into many subintervals that are small enough so that the target function can be replaced by a mean value over the subinterval and taken outside of the integral. Then, a recursion relation can be set up from which the target function emerges as a discrete set of values. Usually, the subintervals chosen are equally spaced on the t axis or on the log t axis. Equation 3 may be expressed as

$$t_n = \sum_{i=1}^{i=n} J(t_{i-1/2})\int_{t_{i-1}}^{t_i} G(t_n - s)\,ds \tag{12}$$

where $J(t_{i-1/2})$ is a suitably determined mean value of $J(t)$ at t between t_{i-1} and t_i; and because $t_i - t_{i-1}$ is chosen to be very small, one may set

$$t_{i-1/2} = (t_i + t_{i-1})/2 \tag{13}$$

Using the definition:

$$d\eta(t_n - s) = -G(t_n - s)\,ds \tag{14}$$

eq 12 may be rewritten as

$$t_n = -\sum_{i=1}^{i=n} J(t_{i-1/2})[\eta(t_n - t_i) - \eta(t_n - t_{i-1})] \tag{15}$$

Separating the $i = n$ term from the sum leads to

$$t_n = J(t_{n-1/2})\eta(t_n - t_{n-1}) -$$
$$\sum_{i=1}^{i=n-1} J(t_{i-1/2})[\eta(t_n - t_i) - \eta(t_n - t_{i-1})] \tag{16}$$

because $\eta(0) = 0$. From the above equation, one obtains the recursion relation

Whole Range of Chain Dynamics

J. Phys. Chem. B, Vol. 109, No. 37, 2005 **17667**

$$J(t_{n-1/2}) =$$

$$\frac{t_n + \displaystyle\sum_{i=1}^{i=n-1} J(t_{i-1/2})[\eta(t_n - t_i) - \eta(t_n - t_{i-1})]}{\eta(t_n - t_{n-1})} \quad \text{for } n > 1 \quad (17)$$

with

$$J(t_{1/2}) = \frac{t_1}{\eta(t_1)} = \frac{2}{G(t_1) + G(0)} \quad (18)$$

as the starting value for $n = 1$. Applying the trapezoidal rule, one may determine $\eta(t_k)$ from

$$\eta(t_k) = \sum_{i=1}^{i=k} \int_{t_{i-1}}^{t_i} G(s)\, ds = \frac{1}{2}\sum_{i=1}^{i=k}[G(t_i) + G(t_{i-1})](t_i - t_{i-1}) \quad (19)$$

If the subintervals are equally spaced on the t axis, to obtain the set of the values $\{J(t_{i-1/2})\}$ using eqs 17 and 19 with $J(t_{1/2})$ given by eq 18 as the start is straightforward. Usually, however, the relaxation of $G(t)$ covers many decades; its values are obtained at equal space on the log t axis. In this case, the $\eta(t_n - t_x)$ quantities ($x = i$, $i - 1$, or $n - 1$) as appearing in eq 17 need to be determined by interpolation from the set of $\eta(t_k)$ values which need first be calculated from eq 19. Preparing the set of $\eta(t_k)$ values for calculating the $\eta(t_n - t_x)$ quantities by interpolation is more straightforward than what is described in ref 23. In calculating the $J(t)$ curves shown in this report, using 10 points per decade in time is sufficient, as no difference can be discerned in the comparisons with curves calculated with a much higher resolution.

Appendix B: Comparison of the K Values Obtained from $G(t)$, $J(t)$, Viscosity, and Diffusion Data

Here, with respect to the frictional factor K, we make a more thorough comparison with the literature data than in ref 6, particularly taking the effect of the finite molecular-weight distribution of the nearly monodisperse samples on their viscosity values into account. The contributions of the $\mu_A(t)$ and $\mu_B(t)$ processes to the viscosity are negligible when the molecular weight is sufficiently high ($> 7\, M_e$). Under such a situation, an analytical expression for the viscosity can be obtained in ERT (see eq 29 of ref 8 or eq 9.24 of ref 5). Using this equation, K can be calculated from the viscosity and density data. The results obtained by Plazek and O'Rourke[29] for samples with $M_w = 0.94\times$, $1.89\times$, and 6.0×10^5 are used in the calculations giving $K = 7.1\times$, $5.9\times$, and 7.7×10^{-9}, respectively, at 127.5 °C, and $3.2\times$, $2.4\times$, and 2.7×10^{-12}, respectively, at 174 °C. It has been shown that the viscosity of a nearly monodisperse sample is slightly larger than that of an ideally monodisperse one with the same (weight-average) molecular weight.[2,5,90] Being for ideal monodispersity, the analytical expression leads to a slightly larger K value as the experimental viscosity value is used in the calculation with the weight-average molecular weight being regarded as the molecular weight in the equation. The bulk of correction can be made to the obtained K value if the M_w/M_n value is known. While being not given, the M_w/M_n values of the three samples can be estimated from matching their measured steady-state compliance J_e^0 values[29] with those calculated from the linear viscoelastic equation, $J_e^0 = \int_0^\infty G(t)t\,dt/(\int_0^\infty G(t)dt)^2$, wherein the $G(t)$ is first calculated from convoluting eq 1 with the Schulz distribution using the polydispersity

parameter Z as the only adjustable parameter. In this way, $Z = 23$, 20, and 10 (correspondingly, $M_w/M_n = 1.04$, 1.05, and 1.1) are obtained for the three samples, respectively. These values are well within the range expected for a nearly monodiperse sample. Then the correction factors for K due to the finite molecular-weight distribution can be obtained by comparing the viscosity results calculated from the analytical equation and from integrating numerically the $G(t)$ which has first been calculated from convoluting eq 1 with the Schulz distribution using the above obtained Z values. In both kinds of calculations the same (weight-average) molecular weight and K are used for each sample. The thus obtained correction factors are 1.24, 1.22, and 1.34 for the three samples, respectively. That the first sample, while having a Z value slightly larger than the second one, has a slightly larger correction factor is due to the fact that at its molecular weight the $\mu_A(t)$ and $\mu_X(t)$ processes can still make a small noticeable contribution to the viscosity. Taking the correction factors into account, the K values are obtained to be $5.7\times$, $4.9\times$, and 5.8×10^{-9}, respectively at 127.5 °C, and $2.6\times$, $2.0\times$, and 2.0×10^{-12}, respectively at 174 °C.

In ref 6, the diffusion proportional constant $K_d = D_G M^2$ determined directly by the diffusion measurements and calculated from the frictional factor $K(K_d = \langle R^2\rangle M_e/3\pi^2 MK)$ obtained from the analyses of the viscoelastic data are compared at 174 °C. The comparison can be equivalently made in terms of K instead of K_d; see ref 6 for the details. From the K_d value (8×10^{-3} cm^2 Da^2/s) of Kramer et al.,[33–35] one obtains $K = 2.5 \times 10^{-12}$ at 174 °C.

The above K values obtained at 127.5 and 174 °C along with those obtained from analyzing the $G(t)$ and $J(t)$ results are listed in Table 1. The K values at 127.5 °C as listed in the first row of the table represent the viscoelastic results of totally 11 samples of different molecular weights ranging from 3.4×10^4 to 6×10^5; the average over these samples with equal weighting is $4.9_3 \times 10^{-9}$ with a standard deviation of 10%, which is basically the same statistically as the average listed in the first row. In the same series of samples whose $G(t)$ results were analyzed, a sample with a molecular weight just above M_e ($M_w = 1.67 \times 10^4 = 1.24 M_e$) gives $K = 4.0 \times 10^{-9}$, which is about 20% lower than the above average value. Considering the fact that the molecular weight of this particular sample is so close to M_e and that any small amount of the components in its molecular-weight distribution having molecular weight smaller than M_e has the effect to reduce the obtained K value somewhat, this deviation, though greater than the standard deviation by a factor of ~ 2, is very consistent with the results of other samples. If this sample is included in the statistical analysis, the average is $4.85 \times 10^{-9} \pm 11\%$. The results listed in Table 1 and discussed above clearly show that the K values obtained independently from different kinds of measurements ($G(t)$, $J(t)$, viscosity, and diffusion) are quantitatively consistent and that the constancy of K extends to the molecular weight as low as just above M_e.

References and Notes

(1) Ferry, J. D. *Viscoelastic Properties of Polymers*, 3rd ed.; Wiley: New York, 1980.

(2) Lin, Y.-H. *Macromolecules* **1986**, *19*, 159.

(3) Lin, Y.-H. *Macromolecules* **1986**, *19*, 168.

(4) Lin, Y.-H. Lin *Macromolecules* **1987**, *20*, 885.

(5) Lin, Y.-H. *Polymer Viscoelasticity: Basics, Molecular Theories, and Experiments*; World Scientific: Singapore, 2003.

(6) Lin, Y.-H. *Macromolecules* **1991**, *24*, 5346.

(7) Doi, M.; Edwards, S. F. *J. Chem. Soc., Faraday Trans. 2* **1978**, *74*, 1789; **1978**, *74*, 1802.

(8) Lin, Y.-H. *Macromolecules* **1984**, *17*, 2846.

(9) Note: In this paper, the term "rubber(like)-to-fluid" is often used to indicate the time region where the description in terms of ERT is applicable. The time region where ERT is applicable is technically slightly different between the line-shape analysis of $G(t)$ and that of $J(t)$. The difference arises from the fact that the $J(t)$ time region which corresponds to the Rouse−Mooney rubber region in $G(t)$ (the $\mu_A(t)$ process region) is much affected or "contaminated" by the glassy-relaxation process $A_G\mu_G(t)$ as shown in Figure 5. Thus, while in $G(t)$ the line shape of the rubber-to-fluid region is uniquely analysed in terms of ERT, in $J(t)$ only the rubberlike-to-fluid region is independently analysed in terms of ERT. Thus in rubber(like)-to-fluid, the term "rubber" is meant for $G(t)$, while "rubber-like" is meant for $J(t)$. Since the frictional factor K is determined by the dynamics in the rubberlike-to-fluid region, the frictional factor K values obtained from $G(t)$ and $J(t)$ as shown in Table 1 are independent of each other. However, the glassy-relaxation process extracted from $J(t)$ as shown in this study is based on the information of the $\mu_A(t)$ process obtained from the $G(t)$ line-shape analysis. Thus, when the term "rubber(like)" is used for $J(t)$, it means that the information of the $\mu_A(t)$ process obtained from the $G(t)$ line-shape analysis (i.e., eq 8) has been used when the $J(t)$ line-shape analysis over the whole range is being made, whose results are shown in Figures 1 and 2.

(10) Ballard, D. G. H.; Rayner, M. G.; Schelten, J. *Polymer* **1976**, *17*, 349.

(11) Norisuye, T.; Fujita, H. *Polym. J.* **1982**, *14*, 143.

(12) Inoue T.; Okamoto, H.; Osaki, K. *Macromolecules* **1991**, *24*, 5670.

(13) Inoue, T.; Hayashihara, H.; Okamoto, H.; Osaki, K. *J. Polym. Sci., Part B: Polym. Phys.* **1992**, *30*, 409.

(14) (a) Inoue, T.; Osaki, K. *Macromolecules* **1996**, *29*, 1595. (b) Inoue, T.; Uematsu, T.; Osaki, K. *Macromolecules* **2002**, *35*, 820.

(15) Lin, Y.-H. *J. Polym. Res.* **1994**, *1*, 51.

(16) Lin, Y.-H.; Lai, C. S. *Macromolecules* **1996**, *29*, 5200.

(17) Lai, C. S.; Juang, J.-H.; Lin, Y.-H. *J. Chem. Phys.* **1999**, *110*, 9310.

(18) (a) Lin, Y.-H.; Luo, Z.-H. *J. Chem. Phys.* **2000**, *112*, 7219. (b) Lin, Y.-H. *J. Chin. Chem. Soc.* **2002**, *49*, 629.

(19) Plazek, D. J. *J. Phys. Chem.* **1965**, *69*, 3480.

(20) Plazek, D. J. *J. Polym. Sci., Part A-2: Polym. Phys.* **1968**, *6*, 621.

(21) Note: The polydispersity of the sample, even though nearly monodisperse, has an effect on the detailed line shape of $J(t)$ in the rubber-like-to-fluid region. This effect, as can be easily accounted for by convolution with the Schulz distribution, virtually does not affect the obtained K value. See section 3.4.

(22) (a) Hopkins, I. L.; Hamming, R. W. *J. Appl. Phys.* **1957**, *28*, 906. (b) Hopkins, I. L.; Hamming, R. W. *J. Appl. Phys.* **1958**, *29*, 742.

(23) Tschoegl, N. W. *The Phenomenological Theory of Linear Viscoelastic Behavior*; Springer-Verlag: Berlin, 1989.

(24) Mooney, M. *J. Polym. Sci.* **1959**, *34*, 599.

(25) Doi, M. *J. Polym. Sci., Part B: Polym. Phys.* **1980**, *18*, 1005.

(26) Note: the relaxation times in the Rouse−Mooney rubber region (τ_A^p) are proportional to K', which is in turn proportional to K through eq 8.

(27) Schulz, G. V. *Z. Physik. Chem., Abst. B* **1943**, *43*, 25; Tung, L. H. *Polymer Fractionation*; Cantow, M. J. R., Ed.; Academic: New York, 1967.

(28) The uncertainty ±0.4 in temperature is estimated from the standard deviation of K as shown in Table 1 and the temperature dependence of viscosity as given in ref 29; this uncertainty is an overestimate as the standard deviation of K includes the errors in molecular weight of the samples.

(29) Plazek, D. J.; O'Rourke, V. M. *J. Polym. Sci. Part A-2: Polym. Phys.* **1971**, *9*, 209.

(30) In the visual superposition to obtain a good fit, both the calculated and measured curves are first displayed in separate figures using the same scales. The figures are stored in a graphic software (CorelDRAW), which allows the superposition to be done under a large magnification on a monitor and at the same time allows the data points being plotted onto the calculated curve. The finished figures can be adjusted to any suitable size. In this procedure, logical steps can be followed to ensure that the comparison between the theory and experiments is accurate.

(31) Lin, Y.-H. *J. Phys. Chem. B* **2005**, *109*, 17670.

(32) Note: Confirmation is made by the agreement between temperature dependence of the structural relaxation time τ_S of sample A as defined in ref 31 (i.e., equivalent to the temperature dependence of the product of K and s) and that of $J(t)$ in the recoverable region determined by Plazek through data reduction, as shown in Figure 5 of ref 31. The agreement in temperature dependence between the obtained K values and the viscosity results of Plazek is also shown in the same figure. These agreements support the consistency between the composition of the $J(t)$ curves measured at different temperatures as shown in Figure 1 and that shown in Figure 2 of ref 19; the former is guided by the fittings to eqs 1, 4, and 5, while the latter was done through the data reduction by Plazek.

(33) Mills, P. J.; Green, P. F.; Palmstrom, C. J.; Mayer, J. W.; Kramer, E. J. *Appl. Phys. Lett.* **1984**, *45*, 958. The measurement temperature 170 °C in this paper has been corrected to be 174 °C in ref 35.

(34) Green, P. F.; Palmstrom, C. J.; Mayer, J. W.; Kramer, E. J. *Macromolecules* **1985**, *18*, 501.

(35) Green, P. F.; Kramer, E. J. *Macromolecules* **1986**, *19*, 1108.

(36) Plazek, D. J. *J. Rheol.* **1996**, *40*, 987.

(37) Note: The blend solution is a binary blend consisting of one nearly monodisperse component with molecular weight much higher than M_e and another with molecular weight just below M_e, which can be regarded as a solvent as far as entanglement is concerned. The details can be found in refs 4 and 5.

(38) Fetters, L. J.; Lohse, D. J.; Richter, D.; Witten, T. A.; Zirkel, A. *Macromolecules* **1994**, *27*, 4639.

(39) Angell, C. A. *Science* **1995**, *267*, 1924 and references therein.

(40) Debenedetti, P. G.; Stillinger, F. H. *Nature* **2001**, *410*, 259.

(41) Plazek[20] estimated that T_g of sample B is lowered by the presence of residual plasticizers by about 1°. Although in general there is some uncertainty as to the measurement of the calorimetric T_g value, the value of sample A should be close to 97 °C, while that of sample B should be around 98.5 °C. (see refs 42 and 43).

(42) Fox, T. G.; Loshaek, S. *J. Polym. Sci.* **1955**, *15*, 371.

(43) Lin, Y.-H. *Macromolecules* **1990**, *23*, 5292 and unpublished results.

(44) Nemoto, N.; Odani, H.; Kurata, M. *Macromolecules* **1972**, *5*, 531.

(45) Note: One may also calculate the shift $\Delta \log t$ using eq 3 of ref 44.

(46) Ninomiya, K.; Ferry, J. D. *J. Phys. Chem.* **1963**, *67*, 2292.

(47) Onogi, S.; Masuda, T.; Kitagawa, K. *Macromolecules* **1970**, *3*, 109.

(48) Plazek, D. J. *Polym. J.* **1980**, *12*, 43.

(49) Okamoto, H.; Inoue, T.; Osaki, K. *J. Polym. Sci.. Part B: Polym. Phys.* **1995**, *33*, 417.

(50) Inoue, T.; Hwang, E. J.; Osaki, K. *J. Rheol.* **1992**, *36*, 1737.

(51) Adachi, K.; Hirano, H. *Macromolecules* **1998**, *31*, 3958.

(52) Doi, M.; Edwards, S. F. *The Theory of Polymer Dynamics*; Oxford University Press: New York, 1986.

(53) Lin, Y.-H. *Macromolecules* **1987**, *20*, 3080.

(54) Sillescu, H. *J. Non-Cryst. Solids* **1999**, *243*, 81 and references therein.

(55) Hempel, E.; Hempel, G.; Hensei, A.; Schick, C.; Donth, E. *J. Phys. Chem. B* **2000**, *104*, 2460.

(56) Tracht, U.; Wilhelm, M.; Heuer, A.; Feng, H.; Schmidt-Rohr, K.; Spiess, H. W. *Phys. Rev. Lett.* **1998**, *81*, 2727.

(57) Cicerone, M. T.; Blackburn, F. R.; Ediger, M. D. *J. Chem. Phys.* **1995**, *102*, 471.

(58) Arndt, M.; Stannarius, R.; Groothues, E.; Hempel, E.; Kremer, F. *Phys. Rev. Lett.* **1997**, *79*, 2077.

(59) Note: Strictly speaking, the fluid region of sample A at 97 °C is slightly affected by the glassy-relaxation process, as show in Figure 1. The effect is more prone to occur as the molecular weight is smaller and the temperature is closer to T_g. In the case of sample A, whose molecular weight is not that low, the effect causes at most a shift of 20% along the time coordinate in the fluid region. Besides, the shift is accounted for in determining the K value as shown by the close fitting between the calculated and measured curves. Thus, any error that can arise is really very small.

(60) Thirumalai, D.; Mountain, R. D. *Phys. Rev. E* **1993**, *47*, 479.

(61) Angell, C. A. *J. Phys. Chem. Solids* **1988**, *49*, 863.

(62) Stillinger, F. H. *J. Chem. Phys.* **1988**, *89*, 6461.

(63) Donati C.; Glotzer, S. C.; Poole, P. H.; Kob, W.; Plimpton, S. J. *Phys. Rev. E* **1999**, *60*, 3107.

(64) Weeks, E. R.; Crocker, J. C.; Levitt, A. C.; Schofield, A.; Weitz, D. A. *Science* **2000**, *287*, 627.

(65) Cicerone, M. T.; Ediger, M. D. *J. Chem. Phys.* **1995**, *103*, 5684.

(66) Cicerone, M. T.; Ediger, M. D. *J. Chem. Phys.* **1996**, *104*, 7210.

(67) Schiener, B.; Bohmer, R.; Loidl, A.; Chamberlin, R. V. *Science* **1996**, *274*, 752.

(68) Richert, R. *J. Phys. Chem. B* **1997**, *101*, 6323.

(69) Russell, E. V.; Israeloff, N. E. *Nature* **2000**, *408*, 695.

(70) Tracht, U.; Wilhelm, M.; Heuer, A.; Feng, H.; Schmidt-Rohr, K.; Spiess, H. W. *Phys. Rev. Lett.* **1998**, *81*, 2727.

(71) Adam, G.; Gibbs, J. H. *J. Chem. Phys.* **1965**, *43*, 139.

(72) Mountain, R. D. *J. Chem. Phys.* **1995**, *102*, 5408 and references therein.

(73) McCrum, N. G.; Read, R. E.; Williams, G. *Anelastic and Dielectric Effects in Polymeric Solids*; Dover: Mineola, NY, 1991.

(74) Kovacs, A. J. *J. Polym. Sci.* **1958**, *30*, 131.

(75) Goldstein, M. *J. Chem. Phys.* **1969**, *51*, 3728.

(76) Moynihan, C. T.; Schroeder, J. *J. Non-Cryst. Solids* **1993**, *160*, 52.

(77) Sastry, S.; Debenedetti, P. G.; Stillinger, F. H. *Nature* **1998**, *393*, 554.

(78) Schroder, T. B.; Sastry, S.; Dyre, J. C.; Glotzer, S. C. *J. Chem. Phys.* **2000**, *112*, 9834.

(79) (a) Fulcher, G. S. *J. Am. Chem. Soc.* **1925**, *8*, 339, 789. (b) Tammann, G.; Hesse, G. *Z. Anorg. Allg. Chem.* **1926**, *156*, 245.

(80) Williams, M. L.; Landel, R. F.; Ferry, J. D. *J. Am. Chem. Soc.* **1955**, *77*, 3701.

(81) Fujara, F.; Geil, B.; Sillescu, H.; Fleischer, G. *Z. Phys. B: Condens. Matter* **1992**, *88*, 195.

(82) Cicerone, M. T.; Ediger, M. D. *J. Phys. Chem.* **1993**, *97*, 10489.

(83) Kind, R.; Liechti, N.; Korner, N.; Hulliger, J. *Phys. Rev. B* **1992**, *45*, 7697.

(84) Swallen, S. F.; Bonvallet, P. A.; McMahon, R. J.; Ediger, M. D. *Phys. Rev. Lett.* **2003**, *90*, 015901.

(85) (a) Ngai, K. L.; Plazek, D. J. *Rubber Chem. Technol.* **1995**, *68*, 376. (b) Plazek, D. J.; Zheng X. D.; Ngai, K. L. *Macromolecules* **1992**, *25*, 4920. (c) Ngai, K. L.; Plazek, D. J. *Macromolecules* **2002**, *35*, 9136.

(86) Lin, Y.-H.; Juang, J.-H. *Macromolecules* **1999**, *32*, 181.

(87) Note: ERT is quantitatively valid only for nearly monodisperse systems. Because of the so-called tube dilation effect which has been shown to occur in the long-time region of a binary blend, ERT will gradually become not applicable when the polydispersity M_w/M_n of the sample has gone significantly beyond 1.1. See refs 5 and 88 for details.

(88) Lin, Y.-H. *Macromolecules* **1989**, *22*, 3075; 3080.

(89) Angell, C. A. *J. Non-Cryst. Solids* **1991**, *131−133*, 13.

(90) See page 182 of ref 5.